Prepared for submission to JCAP

arXiv:1511.07989v4 [astro-ph.CO] 24 Oct 2016

Beyond the standard ΛCDM cosmology: the observed structure of DM halos and the shape of the power spectrum

M. Demiański[a,b] **A.G. Doroshkevich**[c,d]

[a]Institute of Theoretical Physics, University of Warsaw, 02-093 Warsaw, Poland
[b]Department of Astronomy, Williams College, Williamstown, MA 01267, USA
[c]Lebedev Physica Institute of Russian Academy of Sciences,117997, Moscow, Russia
[d]National Research Center Kurchatov Institute, 123182, Moscow, Russia

E-mail: Marek.Demianski@fuw.edu.edu, dorr@asc.rssi.ru

Abstract. Recent advances in observational astronomy allow to study various groups of Dark Matter (DM) dominated objects from the dwarf spheroidal (dSph) galaxies to clusters of galaxies that span the mass range from $10^6 M_\odot$ to $10^{15} M_\odot$. To analyze data of this divers collection of objects we used a simple toy model of spherical DM halo formation that was initially proposed by Peebles. This model introduced the concept of the epoch or redshift of halo formation. Using this concept we analyzed the observational data and revealed correlations between the virial mass, M_{vir}, of halos and basic parameters of their cores, namely, the mean DM density, pressure and entropy. These correlations indicate a high degree of self similarity of both the process of halos formation and their internal structure.

We confirmed the CDM–like shape of both the small and large scale power spectrum. However our reconstruction of the evolutionary history of observed objects differs from expectations of the standard ΛCDM cosmology and requires either a multicomponent composition of DM or a more complex primordial power spectrum of density perturbations with significant excess of power at scales of clusters of galaxies and larger. We demonstrated that a model with suitable combination of the heavy DM particles (CDM) and DM particles with large damping scale (HDM) could provide a successful description of the observational data in a wide range of masses.

Keywords: cosmology: formation of DM halos, galaxies and clusters of galaxies – initial power spectrum – composition of dark matter.

1 Introduction

Observations of the CMB fluctuations by the WMAP mission and ground based telescopes established the ΛCDM model as the best cosmological model (Bennet et al. 2003; Komatsu 2011; Larson 2011; Saro 2014). This inference was supported by the Planck measurements (Ade et al. 2016), observations of clusters of galaxies (see, e.g., Burenin & Vikhlinin 2012) and baryonic acoustic oscillations (Eisenstein & Hu 1998; Meiksin et al. 1999; Samushia et al., 2014). These observations are consistent with the present day theoretical expectations (Ellis et al. 2016; see, however, Rubakov 2014) but other important problems remain unsolved. Thus we do not know the composition and basic properties of dark matter (DM) and dark energy, and we have no information about the possible "missing" cosmological parameters that allow to combine the complex small scale spatial matter distribution with the surprisingly high apparent spherical symmetry and large scale homogeneity of the observed Universe.

Indeed, attempts of direct detection of DM particles by DAMA (Bernabei 2010), CRESST-II (Angloher et al. 2013), and SuperCDMS (Agnese 2014) experiments and other (see reviews in Mayet et al., 2016; Blennow 2016) have not yet produced reliable positive results. Hence up to now we have no reliable estimates of the mass, the nature and properties of DM particles (see, e.g., Blinnikov 2014; Abdallah et al., 2015; Buchmueller et al. 2015; Borsanyi et al., 2016).

Now the main hope of identifying the DM composition is based on the recent progress in observations of objects at high redshifts (Robertson et al. 2015; McLeod 2015; Bouwens et al. 2015a,b; Mitra et al. 2015; Zitrin, 2015) and on observations of Large Scale Structure elements with a size up to 1700 Mpc (see, e.g., Einasto 2014; Balazs et al. 2015; Horvath et al. 2015). These observations are connected with the unexpected properties of the initial perturbations and, so, both with the inflation models and interpretation of the CMB observations (see, e.g. discussions in Demiański & Doroshkevich 2007; Doroshkevich & Verkhodanov 2011).

Results of observations of the small scale structure of the Universe are not so crucial and they require only moderate corrections of the present day models (see review of Berezinsky et al., 2014). Thus the emerging conflict between the Standard ΛCDM model and observations of clustering on subgalactic scales is widely discussed. It is believed that the standard ΛCDM model predicts an excess of low–mass satellites of galaxies similar to the Milky Way (missing satellite problem, see, e.g., Moore et al. 1999; Klypin et al. 1999; Bovil & Ricotti 2009; Trujillo-Gomez et al. 2011). Simulations show that this problem does not appear in the WDM models which however cannot reproduce other observations and so cannot be considered as the basic cosmological model. In this paper we show (Sec.7) that this problem is alleviated in the models with more complex power spectrum of density perturbations.

The core–cusp problem is seen as a discrepancy between the observed and simulated shape of the density profiles in central regions of relaxed objects (see, e.g., Bovill & Ricotti, 2009; Koposov et al., 2009; Walker & Penarrubia, 2011; Boylan- Kolchin et al., 2012; Penarrubia et al 2012; Governato et al. 2012; Sawala, 2013; Teyssier et al. 2013; Laporte et al. 2013; Collins et al. 2014). Significance of these tensions is quite moderate as objects with very different masses, densities and evolutionary histories are compared (see, e.g., Penarrubia et al. 2008). In fact properties of simulated objects are determined using averaged characteristics (density, velocity dispersion etc.) of DM component while the same properties of observed galaxies are derived from measurements of velocities of limited number of stars.

Evidently simulated DM profiles and observed profiles marked by stars are not identical.

First of all observed profiles are distorted by the impact of baryonic components observed as the discs of galaxies or the central galaxies and strong condensation of cooled baryons in clusters of galaxies. To reduce the impact of baryonic component we used in our analysis objects with limited impact of baryons (dSph and ultra diffused galaxies (UDG), small fraction of groups and clusters of galaxies, perhaps, some of LSB galaxies). Secondly the process of formation of stars is sensitive to heating and cooling of the gaseous component, to dissipation of macroscopic turbulent motions and so on. In particular these factors are responsible for the formation of discs, bulges, clusters of stars and other elements of the complex internal structure of observed galaxies. This means that the phase density and entropy of DM, stars and galaxies are different and so their density profiles cannot be identical. More detailed discussion is presented in Sec. 2.

Limited reliability of both these contradictions is enhanced by the limited number of observations and simulations (see, e.g., Mikheeva, Doroshkevich, Lukash 2007; Doroshkevich, Lukash & Mikheeva 2012; Pilipenko et al. 2012; Newman et al. 2013; Brook et al., 2014; Miller et al. 2014; Brooks & Zolotov 2014; Breddels & Helmi 2014; Nipoti & Binney, 2015; Mamon et al. 2015). Among the discussed discrepancies the 'Too Big to Fail' (TBTF) problem (Boylan-Kilchin et al. 2012; Tollerud et al. 2014; Garrison-Kimmel 2014a,b; Klypin et al. 2015) is the most reliable and important. It is discussed in section 7.2 in more details.

Other possible corrections of the standard ΛCDM cosmological model are discussed in the context of small divergences of the local and CMB measurements of the cosmological parameters. Thus emerging tensions between different measurements of the Hubble constant can be explained by introduction of an unstable fraction of DM particles (Berezhiani et al. 2016). The model with unstable DM particles is also discussed by Wang (2014) and Enqvist et al. (2015). These hypotheses reanimate similar earlier proposed models (Turner et al. 1984; Doroshkevich & Khlopov 1984; Doroshkevich et al. 1986, 1988). New observational constrains of possible decay of DM particles are discussed by Baring et al. (2016). Other original models of DM component were discussed by Anderhalsen et al. 2013 and Schewtchenko et al. 2015.

Now the sterile neutrinos with a various masses are widely discussed as the popular candidate for the DM particles (see, e.g., Gorbunov 2014). More popular are the sterile neutrinos in the keV range (see, e.g., reviews of Feng 2010; Boyarsky et al., 2009c, 2013; Kusenko 2009; Marcovič & Viel 2013; Pontzen & Governato 2014; Horiuchi et al., 2015). On the other hand models of light sterile neutrinos are also quite popular (see, e.g., Abazajian 2012; Kopp et al., 2013; Zysina, Fomichev & Khruschov 2014). In some of these complex models sterile neutrinos do not reach the state of thermal equilibrium. A possible decay of sterile neutrinos is also discussed (e.g., Ferrer & Hunter 2013; Bulbul et al. 2014; Enqvist et al. 2015). These models imply a multicomponent composition of DM (Battye & Moss 2014; Whittaker et al. 2014, 2015; Battye et al. 2015; Mirizzi et al. 2015; Abbott 2015). However recently properties of steril neutrinos were strongly constrained by the Ice Cube observations (Aartsen et al. 2016).

Observations of DM dominated halos are very well complemented by numerical simulations that allow to trace and investigate the early stages of halos evolution, as well as the process of halos virialization and formation of their internal structure. The formation of virialized DM halos begins as the anisotropic collapse in accordance with the Zel'dovich theory of gravitational instability (Zel'dovich 1970, Zel'dovich & Novikov, 1983; Demiański et al. 2011). During later stages the evolution of such objects becomes more complex because it is influenced by their anisotropic environment and anisotropic matter inflow (see, e.g., real

cluster representations in Pratt et al. 2009). Moreover all the time the evolution of halos is unavoidably accompanied by the process of violent relaxation and merging, what is also well reproduced by simulations.

Analysis of simulated halos can be performed in a wide range of halo masses and redshifts, what allows to improve the description of properties of relaxed halos of galactic and cluster scales and to link them with the power spectrum of initial perturbations. Thus, it is established that after a period of rapid evolution the main characteristics of majority of the high density DM cores of virialized halos become frozen and their properties are only slightly changing owing to the accretion of diffuse matter and/or the evolution of their baryonic component. The basic properties of the relaxed DM halos in the framework of the ΛCDM model were investigated in many papers (see, e.g., Tasitsiomi et al. 2004; Nagai et al. 2007; Croston et al. 2008; Pratt et al., 2009, 2010; Vikhlinin et al. 2006, 2009; Arnaud et al. 2010; Klypin et al. 2011; Kravtsov & Borgani 2012; Ruffini et al. 2015).

Properties of halos formed by collisionless DM particles are determined by the process of violent relaxation only what leads to the self similarity of the internal structure of halos and implies that halo properties, cosmological evolution and initial perturbations are correlated. Thus for the WDM model the available simulations (see, e.g., Maccio 2012, 2013; Angulo, Hahn, Abel, 2013; Schneider, Smith & Reed, 2013; Wang et al. 2013; Libeskind et al. 2013; Marcovič & Viel 2013; Schultz et al. 2014; Schneider et al. 2014; Dutton et al. 2014) show that in accordance with expectations the number of low mass halos decreases and the central cusp in the density profile is transformed into the core. For larger halos the standard density profile is formed again but formation of high density objects is accompanied by appearance of some unexpected phenomena. Thus Maccio et al. 2012 & 2013, Schneider et al. 2014 confirm the decrease of matter concentration in halos in the WDM model in comparison with the CDM model but they conclude that the 'standard' WDM model is not able to reproduce the density profiles of low mass galaxies. This inference is enhanced by Libeskind et al. 2013, where in contrast with the CDM model their simulation with 1 keV WDM particles cannot reproduce the formation of the Local Group. In turn, Schultz et al. 2014 note that in their simulations with 3keV WDM particles formation of objects at large redshifts and reionization are over suppressed. This means that the simulations of WDM and possibly the multicomponent DM models require further detailed analysis and it is necessary to put special attention to reproduce links between the mass function of halos and the power spectra with the free streaming cut-off.

Without doubt, one can expect a rapid progress in simulations of more complex models of the process of structure formation. However for preliminary discussion of such models we used the semi analytical description of DM dominated objects proposed in our previous paper (Demiański & Doroshkevich 2014). It is based on the approximate analytical description of the structure of collapsed halos formed by collisionless DM particles. During the last fifty years similar toy models have been considered many times in order to study various aspects of the nonlinear process of condensation of matter (see, e.g., Peebles 1967, 1980; Zel'dovich & Novikov 1983; Fillmore and Goldreich 1984; Gurevich & Zybin 1995; Bryan & Norman 1998; Lithwick & Dalal 2011). Of course such models ignore many important features of the process of halos formation and are based on the assumption that a virialized DM halo is formed during a short period of the spherical collapse at $z \approx z_f$ and later on its parameters vary slowly owing to the successive accretion of matter (see, e.g., discussion in Bullock et al. 2001; Diemer et al. 2013; Diemer & Kravtsov 2014).

In this paper we consider observations of DM dominated relaxed objects – dSph and

UDG galaxies and selected sample of 19 clusters of galaxies – in a wide range of their masses, $10^6 \leq M_{vir}/M_\odot \leq 10^{14}$. These data demonstrate the well known correlation between the mass of virialized DM halo M_{vir}, the epoch (or redshift) of its formation, t_f, & z_f, and the corresponding mean DM density, $\langle\rho_{vir}\rangle$. The epoch of galaxies formation was roughly estimated already by Partridge & Peebles 1967a,b. Later on more accurate estimates of this epoch have been discussed in the framework of simple toy models (Zeldovich & Novikov 1983; Lacey & Cole 1993; Bryan & Norman 1998).

Simulations also show that properties of the central cores of virialized DM halos are mainly established during the early period of halos formation and later on the slow pseudo – evolution of cores dominates. This means that they are less sensitive to actions of random factors that distort the outer characteristics of observed objects (see, e.g., Diemer & Kravtsov 2014). This means that analysis of the central properties of DM dominated objects allows to obtain more stable description of virialized objects. However these properties can be distorted by influence of the baryonic component, what makes such analysis more complex.

Our results confirm the self similar character of evolution of the DM dominated objects. Application of the excursion set approach (Press, Schechter 1974; Bardeen et al. 1986; Bond et al. 1991) demonstrates unexpected mass dependence of the amplitude of power spectrum that can be caused by a complex composition of DM particles and/or by a more complex inflationary period.

However potential of this approach should not be overestimated. As usual we can only determine the probability of formation of objects and therefore it has only statistical character rather than strict constrains or prediction. Moreover in our discussion we use observational data of only limited quality and representativity. Thus we can only use a small number of recently observed DM dominated objects, unfortunately their observed characteristics – even so important as the virial mass – are known only with very limited precision and significant scatter. None the less the potential of the proposed approach is significant as it considers objects in a very wide range of masses. We hope that further accumulation of observational data and their comparison with the high resolution simulations will essentially improve presented results.

This paper is organized as follows: In section 2 a simple model of formation of DM halos is presented. In section 3 generation of entropy of DM particles is illustrated and in section 4 an approximate analytical description of properties of DM halos is presented. In section 5 this technique is applied to eight observed samples of DM dominated objects. The mean characteristics of these objects are summarized in Table 1 and are discussed in section 6 . In section 7 the correlation between halo masses and the redshift of formation is compared with expectations of the standard ΛCDM cosmology and the actual shape of the power spectrum is estimated. Discussion and conclusions can be found in section 8 .

1.1 Cosmological parameters

In this paper we consider the spatially flat Λ dominated model of the Universe with the Hubble parameter, $H(z)$, the mean critical density $\langle\rho_{cr}\rangle$, the mean density of non relativistic matter (dark matter and baryons), $\langle\rho_m(z)\rangle$, and the mean density and mean number density of baryons, $\langle\rho_b(z)\rangle$ & $\langle n_b(z)\rangle$, given by Komatsu et al. 2011, Hinshaw et al. 2013:

$$H^2(z) = H_0^2[\Omega_m(1+z)^3 + \Omega_\Lambda], \quad H_0 = 100h\,\mathrm{km/s/Mpc}\,,$$

$$\langle\rho_b(z)\rangle = \frac{3H_0^2}{8\pi G}\Omega_b(1+z)^3 \approx 4\cdot 10^{-31}(1+z)^3\Theta_b\frac{g}{cm^3}\,, \tag{1.1}$$

$$\langle\rho_m(z)\rangle = 2.5\cdot 10^{-30}(1+z)^3\Theta_m\frac{g}{cm^3} = 34(1+z)^3\Theta_m\frac{M_\odot}{kpc^3}\,,$$

$$\langle\rho_{cr}\rangle = \frac{3H^2}{8\pi G},\quad \Theta_m = \frac{\Omega_m h^2}{0.12},\quad \Theta_b = \frac{\Omega_b h^2}{0.02}\,.$$

Here $\Omega_m = 0.24\,\&\,\Omega_\Lambda = 0.76$ are the mean dimensionless density of non relativistic matter and dark energy, $\Omega_b \approx 0.04$ and $h = 0.7$ are the dimensionless mean density of baryons, and the dimensionless Hubble constant measured at the present epoch. Cosmological parameters presented in the recent paper of the Planck collaboration (Ade et al. 2016) slightly differ from those used above.

For this model the evolution of perturbations can be described with sufficient precision by the expression

$$\delta\rho/\rho \propto B(z),\quad B^{-3}(z) \approx \frac{1-\Omega_m+2.2\Omega_m(1+z)^3}{1+1.2\Omega_m}\,, \tag{1.2}$$

(Demiański & Doroshkevich, 1999, 2004, 2014; Demiański et al. 2011) and for $\Omega_m \approx 0.25$ we get

$$B^{-1}(z) \approx \frac{1+z}{1.35}[1+1.44/(1+z)^3]^{1/3}\,. \tag{1.3}$$

For $z = 0$ we have $B = 1$ and for $z \geq 1$, $B(z)$ is reproducing the exact function with accuracy better than 90%. For $z \geq 1$ these relations simplify. Thus, for the Hubble constant and the function $B(z)$ we get

$$H^{-1}(z) \approx \frac{0.85\cdot 10^{18}s}{\sqrt{\Theta_m}(1+z)^{3/2}},\quad B(z) \approx \frac{1.35}{1+z}\,. \tag{1.4}$$

2 Physical model of halos formation

It is commonly accepted that in the course of complex nonlinear condensation the DM forms stable virialized halos with a more or less standard density profile and their typical mass is slowly increasing with time. Numerical simulations show that the virialized DM halos with various masses are formed from initial perturbations after a short period of rapid complex evolution. Such virialized objects are observed as clusters of galaxies, isolated galaxies and/or as high density galaxies within less dense clusters of galaxies, filaments, superclusters or other elements of the Large Scale Structure of the Universe.

Evidently the halo formation is a deterministic process and properties of virialized objects correlate with properties of the initial perturbations. However the complex character of the process of halo formation destroys many correlations and allows to reveal only some of them. The most stable characteristics are the density profile of DM halos and the mean density, pressure and entropy of their cores. It can be expected that these characteristics are moderately distorted in the course of halos formation and subsequent evolution.

Properties of both simulated and observed DM dominated virialized objects – galaxies and clusters of galaxies – are usually described in the framework of spherical models such as the Navarro – Frenk – White (NFW) proposal (Navarro et al. 1995, 1996, 1997; Ludlow et al. 2013), isothermal or Burkert 1995 & 2015 models. This approach allows to discuss and to link together both the general parameters of a halo, such as its mass, period of its formation

and relations between the thermal and gravitational energy, and its internal properties such as the density profile, mean density and entropy of its core etc.

In this paper using this model we consider the observed properties of DM dominated virialized objects – the dSph galaxies and some set of clusters of galaxies – in a wide interval of masses $10^6 \leq M_{vir}/M_\odot \leq 10^{15}$ and we assume that all relaxed DM halos are described by the NFW density profile. Our approach is based on three arguments:

1. all objects are formed from initial perturbations described by the same power spectrum,
2. the internal structure of all halos is determined by the same processes of violent relaxation,
3. many numerical simulations support these inferences.

This approach implies a high degree of self similarity in mass dependence of the main characteristics of DM halos. Of course, it ignores many details of the complex process of halos formation and in particular it does not prevent formation of low mass objects at any redshift. But it allows to obtain a very simple, though rough, general description of the process of DM halos formation and introduces some hierarchy of formed objects.

This analysis also reveals a possible deviations of the main observed characteristics from expectations based on standard assumptions about the DM composition and/or initial power spectrum used in theoretical models and simulations. An example of such deviation is the 'To Big to Fail' effect (Boylan–Kolchin et al. 2012; Garrison–Kimmel et al., 2014a,b; Tollerud et al. 2014; Klypin et al. 2015; Hellwing et al. 2015; Brook, & Cintio 2015) what indicates that the usually accepted models should be improved.

2.1 DM density in virialized halos

In this paper we assume that all relaxed DM halos, under consideration, are described by the NFW density profile

$$\rho(x) = \frac{\rho_0}{x(1+x)^2}, \quad x = r/r_s\,, \tag{2.1}$$

where $\rho_0(M_{vir})$, & $r_s(M_{vir})$ are model parameters. Using this density we get that

$$M(r) = M_s f_m(r/r_s), \quad M_s = 4\pi\rho_0 r_s^3, \quad M_{vir} = M_s f_m(c)\,,$$

$$f_m(x) = ln(1+x) - x/(1+x), \quad c = R_{vir}/r_s \geq 3\,, \tag{2.2}$$

$$M(r_s) = M_s f_m(1) \approx 0.2 M_s\,,$$

where c is the concentration and R_{vir} is the halo virial radius. For the mean density of halos, $\langle\rho_{vir}\rangle$ and the mean density of their central core $\langle\rho_s\rangle$ we get

$$\langle\rho_{vir}\rangle = 3M(R_{vir})/4\pi R_{vir}^3 = 3\rho_0 f_m(c)/c^3\,,$$

$$\langle\rho_s\rangle = 3M(r_s) f_m(1)/4\pi r_s^3 \approx 0.6\rho_0\,,$$

and finally we have

$$\langle\rho_s\rangle = 5.4\langle\rho_{vir}\rangle \left(\frac{c}{3}\right)^3 \frac{1}{f_m(c)}\,. \tag{2.3}$$

2.2 The redshift of halo formation

For each mass of DM halo its formation is a complex process extended in time what causes some ambiguity in the halo parameters such as its virial mass and the epoch or redshift of formation (see, e.g. discussion in Partridge & Peebles 1967a,b; Peebles 1980; and more recently in Diemand, Kuhlen & Madau 2007; Kravtsov & Borgani 2012). The main stages of this process can be investigated in details with numerical simulations (see, e.g. Demiański et al. 2011). The analytic description of this process is however problematic.

For a virialized DM halo of mass M_{vir} the redshift (or epoch) of formation, z_f, and the corresponding mean DM density $\langle\rho_{vir}\rangle$ were roughly estimated by Partridge & Peebles 1967a,b and were later determined more accurately in the framework of the simple *phenomenological* toy models (Zeldovich & Novikov 1983; Lacey & Cole 1993; Bryan & Norman 1998). According to these models the virial density is proportional to the mean density (1.1) at the moment of object formation,

$$\langle\rho_{vir}\rangle = 18\pi^2\langle\rho_m(z_f)\rangle \approx \rho_{200}(1+z_f)^3\,, \tag{2.4}$$

$$\rho_{200} = 200\langle\rho_m(0)\rangle = 0.68\cdot 10^4 M_\odot/kpc^3 = 5\cdot 10^{-28} g/cm^3.$$

In the Lacey – Cole model halos are considered as formed at the moment of collapse of homogeneous spherical DM clouds and they are described by the adiabatic Emden model with $\gamma = 5/3$, $n = 3/2$ (Peebles 1980; Zel'dovich & Novikov 1983).

The advantage of this approach is its apparent universality and reasonable results that are obtained for massive clusters of galaxies. However both its precision and range of applicability are limited owing to noted simplified assumptions. Thus even the numerical coefficient $18\pi^2$ is determined by the Emden model for halo description. An important, but usually ignored, special feature of the Lacey - Cole model is the strong mass dependence of the virial density,

$$\langle\rho_{vir}\rangle \propto M_{vir}^{-2}\,. \tag{2.5}$$

Attempts to use these relations for unified description of observed DM halos of galactic and clusters scales immediately leads to strongly unacceptable results. Thus expectations of the model (2.4, 2.5) are in contrast with the weak mass dependence of the observed parameters of DM dominated objects (sections 5 & 6). It is also important that for dSph galaxies Eq. (2.4) leads to a very high value of $z_f \sim 15$, what exceeds both the age of dSph galaxies derived from observations of stars (see, e.g., Weisz et al. 2014; Karachentsev et al., 2015) and the redshift of reionization $z_{reio} \sim 9$ determined by Planck (Ade 2016). Non the less the main significance of the Lacey – Cole model (2.4) is the clear introduction of the concept of the epoch (or redshift z_f) of halo formation, what allows us to quantify correlation of halo parameters with the process of growth of perturbations and halo formation.

Evidently the basic assumptions of the simple model (2.4) are not realistic. Indeed the real halos are formed successively beginning from the core, what increases $\langle\rho_{vir}\rangle$ as compared with (2.4). Further on the processes of merging and anisotropic matter accretion unpredictably changes the density. Analysis of high resolution simulations (Demiański et al. 2011) shows that influence of these random factors together with the strong anisotropy of the early period of DM halo formation depends upon the halo mass and, for example, it is moderate for clusters of galaxies within which earlier formed galaxies are observed as separate very dense elements. It is accepted that for the simple ΛCDM cosmological model and for

more massive objects the expression (2.4) describes reasonably well both the observations and simulations. However as is discussed in section 3 the formation of low mass objects is regulated by other factors and thus their structure cannot be described by the same relations. These comments attempt to explain the main reasons why the model (2.4, 2.5) has limited applicability.

In order to describe the complex process of DM halo formation in a wide range of virial masses of objects we use the more general *phenomenological* relation

$$\langle\rho_{vir}\rangle = 18\pi^2\Phi(M_{vir})\langle\rho_m(z_f)\rangle \approx \rho_{200}\Phi(M_{vir})(1+z_f)^3/,, \tag{2.6}$$

where $\Phi(M_{vir}) \geq 1$ is a smooth slowly varying function of M_{vir}. This relation preserves the universality of (2.4) and provides an unified self consistent description of observed properties of DM halos in a wide range of masses $10^6 \leq M_{vir}/M_\odot \leq 10^{15}$. In particular, it reproduces the observed weak mass dependence of the redshift z_f and the density $\langle\rho_{vir}\rangle$ for both clusters of galaxies and low mass THINGs, LSB, UDG and dSph galaxies. Further discussion of these problems can be found below in sections 4, and 5 .

The expression (2.6) allows us to take into account anisotropy of the collapse, what decelerates the process of objects formation and decreases both the virial density and z_f. It can be used in more complex cosmological models (such as, e.g., Nesseris & Sapone, 2015).

Precise observations of DM periphery of both clusters and galaxies are problematic owing to the strongly irregular matter distribution in their outer regions. Hence, we use only estimates of the more stable parameter - the virial mass of object as its leading characteristic. For example, sometimes the relation (2.4) is used for description of clusters of galaxies under the arbitrary assumption that the cluster is formed at the observed redshift, $1+z_f \equiv 1+z_{obs}$. In this case the relation (2.4) allows to determine formally the mean virial density $\langle\rho_{vir}\rangle$ and, for a given mass of cluster M_{vir}, its virial radius, R_{vir}. However this result is evidently incorrect because, in fact, we can only conclude that $z_f \geq z_{obs}$, what is trivial for galaxies. For clusters the difference between $1+z_f$ and $1+z_{obs}$ can be as large as $\sim 1.5-2$.

More stable and refined method to determine the redshift of halo formation uses characteristics of the halo core rather than its periphery. In this case we use the following expression for the concentration

$$c(M_{vir}, z_f) \approx 0.12 M_{12}^{1/6}(1+z_f)^{7/3}, \quad M_{12} = \frac{M_{vir}}{10^{12}M_\odot}, \tag{2.7}$$

(Demiański & Doroshkevich 2014; Ludlow et al. 2016). Together with relations (2.3) and (2.6) we get for the mean density of the central core

$$\langle\rho_s\rangle = \rho_{cc} M_{12}^{1/2}(1+z_f)^{10}\Phi(M_{vir})\,, \tag{2.8}$$

$$\rho_{cc} = 0.38\cdot 10^{-3}\frac{\rho_{200}}{f_m(c)} \approx \frac{2.5}{f_m(c)}\frac{M_\odot}{kpc^3} = \frac{1.9}{f_m(c)}\cdot 10^{-31}\frac{g}{cm^3}\,.$$

This relation links the redshift z_f with the virial mass M_{vir} and the mean density of halo core $\langle\rho_s\rangle$ and allows to determine z_f. Application of this approach requires additional observations. However it is less sensitive to random deviations of characteristics of periphery of objects. Moreover for DM dominated high density objects observed at $z_{obs} \ll 1$ (such as the dSph galaxies) determination of the redshift z_f through the parameters of the central core is also preferred.

The main weakness of this approach is the possible impact of baryonic component that can be specially important for galaxies with moderate DM domination. However for dSph galaxies this effect can be comparable with the uncertainties in measurements of parameters, what is clearly seen when one compares the results presented in Walker et al. 2009 and Kirby et al. 2014 (see sections 5.5 & 5.6).

Comparison of (2.6) and (2.8) indicates that the density of halo core $\langle\rho_s\rangle$ is more sensitive than $\langle\rho_{vir}\rangle$ to both the virial mass and the redshift of formation. However for all observed samples (section 5) there is a correlation between z_f and M_{vir}:

$$\eta_f = (1+z_f)M_{12}^{0.077} \approx 4.1(1\pm0.1)\,, \tag{2.9}$$

(see also Demiański & Doroshkevich 2014). Allowing for this correlation we see from (2.8) that actually $\langle\rho_s\rangle$ is a weak function of both the virial mass M_{vir} and the redshift of formation z_f.

2.3 Excursion set approach and shape of the power spectrum

It is seen from (2.6) that the redshift of halo formation z_f is uniquely related to the mean DM density of the virialized object. As it is demonstrated below sometimes it is more convenient to use this redshift for description of halos. In particular, it is well known that at redshifts $z \geq 3$ the formation of galactic scale halos dominates, but the typical mass of halos increases with time and massive clusters of galaxies are mainly formed later at redshifts $z \leq 2$. This correlation between the redshift of halo formation z_f and the halo mass M_{vir} is described by current models of halo formation.

Majority of such models (Press & Schechter 1974; Bardeen et al. 1986; Bond et al. 1991; Sheth & Tormen 2002; 2004) are based on the excursion set approach applied to the initially Gaussian random density perturbations. They reduce description of characteristics of the formed halos to the problem of crossing of an appropriate barrier by particles undergoing Brownian motion. These problems were discussed very actively at the end of previous century with the use of 2D and 3D simulations with different power spectra and a close link between the power spectrum and properties of DM halos and Large Scale Structure had been demonstrated. The short review of pertinent publications can be found in Sheth & Tormen 2002 & 2004.

Here we apply this approach to the analysis of observed DM dominated objects in a wide range of virial masses ($10^6 \leq M_{vir}/M_\odot \leq 10^{15}$), what allows us to demonstrate unexpectedly complex shape of the function $z_f(M_{vir})$. Possible explanations of this fact are discussed in section 5.

All theoretical models of halos formation predict that the distribution functions of halo characteristics are dominated by a typical Gaussian term:

$$dP(M_{vir}) \propto \exp[-\alpha\Psi^2(M_{vir})]dM_{vir}\,, \tag{2.10}$$

$$\Psi(M_{vir}) = \sigma_m(M_{vir})B(z_f(M_{vir}))\,,$$

where $B(z_f)$ (1.2, 1.4) describes the growth of density perturbations and σ_m is the dispersion of density perturbations and it is given by

$$\sigma_m^2(M) = \frac{1}{2\pi}\int_0^\infty k^2 p(k) W^2(k,M)dk\,. \tag{2.11}$$

Here $p(k)$ is the power spectrum and

$$W(x) = 3(sin\, x/x^3 - cos\, x/x^2), \quad x = kr \propto kM^{1/3}\,,$$

is the Fourier transform of the real-space top-hat filter corresponding to a spherical mass M. Thus, the function $\Psi(M_{vir})$ characterizes the amplitude of perturbations with mass M_{vir}.

The usually used condition

$$\Psi(M_{vir}) = \sigma_m(M_{vir})B(z_f(M_{vir})) \approx const\,, \tag{2.12}$$

provides the expected approximate self similarity of the process of halo formation and progressive growth with time of the virial mass of halos. This model is consistent with the main results of numerous 2D and 3D numerical simulations performed with different box sizes, power spectra and resolution (see, e.g., discussion in Sheth & Tormen 2002).

The coefficient α in (2.10) depends upon the used normalization of σ_m and specifies the universal barrier that discriminates the linear from the nonlinear evolution of a DM halo with the mass M_{vir}. For example, for the CDM – like power spectrum and for the standard normalization of perturbations on σ_8 the function σ_m and α are well fitted by the following expressions

$$\sigma_m = \frac{3.31\sigma_8 M_{12}^{-0.077}}{1 + 0.177M_{12}^{0.133} + 0.16M_{12}^{0.333}}, \quad \alpha = \frac{1.686^2}{2\sqrt{2}} \approx 1\,, \tag{2.13}$$

where $M_{vir} = M_{12}10^{12}M_\odot$, 1.686 is the critical overdensity (height of the barrier) and $\sigma_m \approx \sigma_8$ for

$$M_{12} = \frac{4\pi}{3}\frac{\langle\rho_m\rangle}{10^{12}M_\odot}\left(\frac{8Mpc}{h}\right)^3 \approx 210\Theta_m\left(\frac{0.7}{h}\right)^3\,.$$

Below in section 5 other normalizations of the functions $\Psi(M_{vir})$ and σ_m based on the observed parameters will be used.

It is interesting that for $M_{12} \leq 1$ we get from (1.4), (2.9), and (2.13) that

$$\Psi(M_{vir}) \approx \frac{4.47\sigma_8}{(1+z_f)M_{12}^{0.077}} = 1.1\sigma_8\left(\frac{4.1}{\eta_f}\right) \approx const\,, \tag{2.14}$$

what is consistent with (2.12) and demonstrates that properties of low mass objects are in agreement with the CDM–like shape of the small scale power spectrum. We will discuss in more details the observed properties of the function $\Psi(M_{vir})$ in section 5.

3 The entropy of the relaxed DM halos

Entropy is a very important characteristic of virialized DM halos as it is conserved during their adiabatic evolution. The entropy of a DM halo includes a component related to small scale random perturbations of the compressed matter and a component generated in the course of violent relaxation of the compressed matter. Evidently the former depends directly upon the initial power spectrum while the latter depends mainly upon the halo mass and the period of halo formation.

Simulations demonstrate that indeed in accordance with the Zel'dovich approximation during the early stages of halo formation the very complex anisotropic matter compression

takes place and theoretical description of this period is problematic (see, e.g., detailed discussion in Demiański et al. 2011). Published discussions of the process of violent relaxation (Filmore and Goldrich 1987; Gurevich and Zibin 1995; Lithwick and Dalal 2011; and others) use the simplest spherical models and can illustrate but not reproduce the real complex process of violent relaxation.

Estimates of these components of entropy are given in Appendix A. They can be compared with estimates obtained from the analysis of observed objects.

The model (2.4, 2.5) describes the DM halo formation from a spherical cloud of DM particles at rest, what implies zero initial entropy of the cloud. Thus this model demonstrates that some entropy is really generated within the collapsed and relaxed DM halos even without any initial entropy. This entropy can be roughly estimated as (A.3)

$$\langle S_{vir}(M)\rangle \approx 4.3 M_{12}^{0.74} cm^2 keV \frac{\mu_{DM}^{2/3}}{\Phi^{1/3}} \frac{\eta_f}{4.1} \frac{72}{\theta_{vir}}\,, \tag{3.1}$$

where $\mu_{DM} = m_{DM}/m_b$, $m_{DM}\,\&\,m_b$ are the masses of DM particles and baryons, θ_{vir} is the standard ratio of the gravitational and internal energy of virialized objects averaged over 180 observed clusters with masses $10^{13} \le M_{vir}/M_\odot \le 10^{15}$:

$$\theta_{vir} = \frac{M_{vir}}{10^{12} M_\odot} \frac{1Mpc}{R_{vir}} \frac{1kev}{T_x} \approx 72(1 \pm 0.08)\,, \tag{3.2}$$

and T_x is the measured x-ray halo temperature. This entropy is comparable with observational estimates (6.1). However these estimates apply mainly to peripheries of halos with large entropy.

The second component includes contribution of random motions linked with the random density perturbations. Using the correlation between the redshift z_f and the virial mass of halo (2.9) we get for this component (A.8)

$$S_r(M_{vir}) \approx 6.4 M_{12}^{0.81} \mu^{5/3} g_r (\eta_f/4.1)^3 cm^2 keV\,, \tag{3.3}$$

where g_r is a factor that determines the fraction of random energy accumulated by the halo. This value is also comparable with the observational estimates (6.1).

It can be expected that this channel of entropy generation is more important for less massive halos.

4 Expected properties of the relaxed DM halos

We consider the DM halos as a one parametric sequence of objects all properties of which depend upon their virial mass. This means that we consider all DM halos as similar ones. Together with the virial characteristics of halos, namely, the mass, M_{vir}, radius R_{vir}, and density $\langle\rho_{vir}\rangle$ we also consider the mean characteristics of the central cores, namely, the density $\langle\rho_s\rangle$, pressure, $\langle P_s\rangle$, temperature $\langle T_s\rangle$, entropy $\langle S_s\rangle$ and DM surface density, $\langle\Sigma_s\rangle$. The very important characteristic of a halo is the redshift of its formation, z_f, that was introduced by (2.6), it approximately characterizes the end of the period of halo formation and relaxation.

The DM temperature and velocity dispersion σ_v in the core usually are not observed but within relaxed DM cores σ_v is close to the circular velocity, $v_c(r)$, (Demiański & Doroshkevich 2014)

$$\sigma_v^2(r) \approx v_c^2(r)\sqrt{r_s/r}\,. \tag{4.1}$$

Because of this we can estimate the expected central parameters of a DM halo as:

$$\langle T_s \rangle \approx \frac{m_b v_c^2}{2} \approx 1.8 eV\, M_{12}^{5/6} (1+z_f)^{10/3} (\Phi/f_m)^{1/3} \mu_{DM}\,,$$

$$\langle P_s \rangle \approx 10^{-7} eV/cm^3\, M_{12}^{4/3} (1+z_f)^{40/3} (\Phi/f_m)^{4/3}\,, \tag{4.2}$$

$$\langle S_s \rangle \approx 80 cm^2 keV \frac{M_{12}^{1/2}}{(1+z_f)^{10/3}} \mu_{DM}^{5/3} (f_m/\Phi)^{1/3}\,.$$

Using the correlation between z_f and M_{vir} (2.9) we finally get

$$\langle T_s \rangle \approx 0.2 keV\, M_{12}^{0.6} \left(\frac{\eta_f}{4.1}\right)^{10/3} \left(\frac{\Phi}{f_m}\right)^{1/3} \mu_{DM}\,,$$

$$\langle \rho_s \rangle \approx \eta_\rho M_{12}^{-0.2} \frac{\Phi}{f_m} \left(\frac{\eta_f}{4.1}\right)^{10}\,,$$

$$\langle P_s \rangle \approx \eta_p M_{12}^{0.4} \left(\frac{\Phi}{f_m}\right)^{4/3} \left(\frac{\eta_f}{4.1}\right)^{40/3}\,, \tag{4.3}$$

$$\langle S_s \rangle \approx \eta_s M_{12}^{0.73} \left(\frac{\eta_f}{4.1}\right)^{-10/3} \left(\frac{f_m}{\Phi}\right)^{1/3} \mu_{DM}^{,}\,.$$

where expected values of constants are

$$\eta_\rho \approx 2.6 \cdot 10^6 \frac{M_\odot}{kpc^3}, \quad \eta_p \approx 22 \frac{eV}{cm^3}, \quad \eta_s \approx 0.9 cm^2 keV\,. \tag{4.4}$$

The expected self similar character of the internal structure of DM cores is manifested by a weak dependence of the parameters η_f, η_ρ, η_p, & η_s upon the virial mass of objects in a wide range of masses. For the observed objects these parameters are obtained in the next section and are presented in Table 1. For the best sample of 19 dSph galaxies with $M_{vir} \leq 10^9 M_\odot$ and 19 CLASH clusters with $M_{vir} \geq 10^{14} M_\odot$ we have

$$\eta_\rho \approx 1.3 \cdot 10^6 (1 \pm 0.9) \frac{M_\odot}{kpc^3}, \quad \eta_s \approx 1.2(1 \pm 0.5) cm^2 keV, \quad \eta_f \approx 4.1(1 \pm 0.1)\,, \tag{4.5}$$

what is quite similar to expectations (4.4). Here and below we use the correction factor

$$\Phi(M_{vir}) = (1 + M_f/M_{vir})^{0.3}, \quad M_f \approx 8 \cdot 10^{12} M_\odot\,, \tag{4.6}$$

that allows us to obtain an unified self consistent description of both discussed galaxies and clusters of galaxies. Thus for larger masses $M_{vir} \gg M_f$, $\Phi \to 1$, and expressions (2.4) and (2.6) become identical to each other. On the other hand, in the opposite case $M_{vir} \ll M_f$ the function (4.6) allows to reconcile theoretical expectations (4.3) with observations (6.1) presented in section 5. For low mass dSph galaxies this approach decreases the redshift of formation z_f down to values consistent with the observed age of stars and Planck estimates of the redshift of reionization.

Of course the function $\Phi(M_{vir})$ (4.6) should be considered only as the first approximation. But to obtain more refined and justified description of the redshift of formation z_f (2.6) and DM halo parameters (4.3) we need to have both richer observational data with only moderate scatter and corresponding high resolution simulations.

As is seen from (2.9) and (2.7) the so defined concentration is only weakly depended on the virial mass,

$$\langle c\rangle \approx 3(\eta_f/4.1)^{7/3} M_{12}^{0.004}\,, \tag{4.7}$$

what is confirmed – in the range of data uncertainties – by the results presented in Table 1. It is interesting that from these relations it immediately follows the widely discussed weak mass dependence of the DM surface density of both the core, Σ_s, and the virialized object, Σ_{vir}. Indeed,

$$\langle\rho_{vir}\rangle = 64\rho_{200}\frac{\Phi(M_{vir})}{M_{12}^{0.21}}\left(\frac{\eta_f}{4.1}\right)^3 \approx \frac{45\cdot 10^{-5}}{M_{12}^{0.21}}\left(\frac{\eta_f}{4.1}\right)^3 \Phi\frac{M_\odot}{pc^3}\,,$$

$$\Sigma_{vir} = \langle\rho_{vir}R_{vir}\rangle \approx 35 M_{12}^{0.20}\left(\frac{\eta_f}{4.1}\right)^2 \Phi^{2/3}\frac{M_\odot}{pc^2}\,,$$

$$\Sigma_s = \langle\rho_s r_s\rangle = \frac{\Sigma_{vir}c^2}{5f_m(c)} \approx 65 M_{12}^{0.28}\left(\frac{\eta_f}{4.1}\right)^{6.7} \Phi^{2/3}\frac{M_\odot}{pc^2}\,. \tag{4.8}$$

Such stability of both surface densities Σ_s and Σ_{vir} was discussed in many papers (see, e.g., Spano et al., 2008; Donato et al. 2009; Salucci et al. 2011; Demiański & Doroshkevich 2014; Saburova & Del Popolo, 2014). Estimates of Σ_s (4.8) and that listed in Table 1 are similar to results of Kormendy & Freeman 2015. It supports the expected self similarity of the process of DM halo formation and the proposed description of the halo structure. In particular it supports the proposed modification of the model (2.6).

5 Observed characteristics of DM dominated galaxies and clusters of galaxies

For our analysis we used more or less reliable observational data for $\sim$ 19 DM dominated clusters of galaxies, 30 groups of galaxies, one UDG, $\sim$ 30 dSph, and $\sim$ 11 THINGS and LSB galaxies. The analysis of observations of the dSph galaxies in the framework of accepted model was performed in Demiański & Doroshkevich 2014. Here we improved this analysis and compared the observational results obtained within a wide interval of virial masses with theoretical expectations.

Now there are more or less reliable observational data for at least $\sim$ 300 clusters of galaxies (Pointecouteau et al. 2005; Arnaud et al., 2005; Pratt et al., 2006; Zhang et al., 2006; Branchesi et al., 2007; Vikhlinin et al., 2009; Pratt et al. 2010; Suhada et al. 2012; Moughan et al. 2012; Bhattacharya et al. 2013; Merten et al. 2015). However, usually the central cluster characteristics are not directly observed and are obtained by a rather complex procedure (see, e.g., Bryan & Norman 1998; Pointecouteau et al. 2005; Vikhlinin et al. 2009; Lloyd–Davies et al. 2011; McDonald et al., 2013). In spite of the rapid progress of investigations of clusters of galaxies, recent publications discuss mostly the general cluster characteristics such as their observed redshift z_{obs}, virial mass, M_{vir}, radius, R_{vir}, and average

X-ray temperature, T_x. However in this paper we are mainly interested in discussion of more stable central regions of clusters and, in particular, in concentrations and the central pressure and entropy of DM component. Unfortunately such data are very limited and for our analysis we can use the CLASH survey only. For comparison and in order to demonstrate the possible complex impact of baryonic component we also consider 83 SPT clusters (McDonald et al. 2013).

In this section we consider properties of the central cores of virialized DM halos using the approximation summarized in the previous section. We characterize halos by their virial mass M_{vir} and redshift of formation, z_f. We assume that at $z \leq z_f$ the halos mass and core temperature and density do not change significantly.

5.1 The CLASH clusters

For 19 clusters of the CLASH sample (Merten et al. 2015) in addition to the usually presented observed virial mass of clusters, M_{vir}, there are also estimates of the size and density of central core, r_s, & ρ_0. For this survey the published parameters R_{vir}, & ρ_{vir} are obtained under the assumption that $z_f = z_{obs}$ and they are not used in our analysis. The virial mass of clusters, M_{vir}, presented in Merten et al. 2015 is close to the estimates of M_{vir} obtained by Umetsu et al. 2014, what confirms reliability of these estimates.

It is important that for these clusters parameters of cores can be used without serious corrections and the concentrations $\langle c \rangle \leq 4$ are quite moderate. The similarity of r_s and r_{vir} demonstrates a limited impact of central galaxies and/or cooled baryonic component for these clusters (see, e.g. Mantz 2014) and allows to consider these data as typical among DM dominated clusters. Main results are presented in Table 1 and are plotted in Figs. 1 and 2.

The difference between our estimates of z_f and z_{obs} for this survey

$$\langle (1+z_f)/(1+z_{obs}) \rangle \approx 1.7(1 \pm 0.2)\,, \tag{5.1}$$

demonstrates arbitrary character of the assumption that $z_f \equiv z_{obs}$ and conventional character of results based on this assumption.

Using (A.1) we get for this survey

$$\langle \theta_{vir} \rangle = 77(1 \pm 0.2), \quad \langle M_{12} \rangle = 900(1 \pm 0.3)\,, \tag{5.2}$$

$$\langle \rho_s \rangle = 5 \cdot 10^5 (1 \pm 0.5) M_\odot / kpc^3, \quad \langle 1+z_f \rangle = 2.3(1 \pm 0.1)\,,$$

and for the ΛCDM spectrum (2.13)

$$\langle \Psi(M) \rangle = 0.4\sigma_8 (1 \pm 0.1)\,. \tag{5.3}$$

5.2 The SPT – clusters

For 83 clusters selected by the South Pole Telescope (Reinhardt et al. 2013; McDonald et al. 2013; Ruel et al. 2013; Saliwanchik et al. 2015) the central baryonic density, temperature and entropy are given at radius $r \leq 0.012 R_{500}$ while the expected radius of the cluster core is $r_s \sim (0.15 - 0.25) R_{500}$. For these clusters also the standard virial masses M_{500} are known but no information on the DM component is provided, what prevents us to reconstruct accurately parameters of these cores. However these clusters nicely illustrate the complex behavior of their baryonic cores.

This sample is clearly divided into two groups with different properties of their observed baryonic component. One of them contains 35 clusters with baryonic number density $\langle n_b \rangle \geq$

$8 \cdot 10^{-3} cm^{-3}$ and entropy of the central core $\langle S_b \rangle \leq 90 cm^2 keV$, what indicates the noticeable cooling of the baryonic component. Owing to the thermal instability this process results in the formation of two component medium – cold low mass high density baryonic subclouds within hot low density diffuse baryonic gas (Doroshkevich & Zel'dovich 1981). In these clusters the observed density relates to the denser fraction while the observed temperature relates to the diffuse hot gas and random velocities of clouds (see, e.g., Khedekar et al. 2013; Battaglia et al., 2015; Adam et al., 2015). This means that for these clusters the real central pressure and entropy of the hot baryonic component are close to that measured for the hotter subsample of clusters.

The hotter group contains 38 clusters with baryonic entropy

$$\langle S_b \rangle = 270(1 \pm 0.5) cm^2 keV\,.$$

Unfortunately we have no information about the central characteristics of their DM component. However if we assume that in central regions

$$\langle \rho_{DM} \rangle \approx 3 \langle \rho_b \rangle\,, \tag{5.4}$$

then our estimates of cluster characteristics become close to (5.2) and (5.3). This choice seems to be quite reasonable. Indeed for intercluster medium we expect that $\langle \rho_m \rangle / \langle \rho_b \rangle \approx 6$, see (1.1). In clusters the baryonic component tends to cool and to settle in their cores, what decreases the ratio $\langle \rho_m \rangle / \langle \rho_b \rangle$. For these 38 clusters with the accepted value of (5.4) the mean results are quite similar to those obtained for the CLASH survey, in particular,

$$\langle (1 + z_f) \rangle = 2.9(1 \pm 0.1), \quad \langle \Psi(M) \rangle = 0.34 \sigma_8 (1 \pm 0.1)\,. \tag{5.5}$$

5.3 The groups of galaxies

30 suitable groups of galaxies with $z_{obs} \ll 1$, masses $1.2 \leq M_{12} \leq 200$ and sizes $100 kpc \leq R \leq 700 kpc$ are taken from the catalog of Makarov & Karachentsev 2011. For these objects we cannot separate the central core and estimate its parameters. But these data allow us to estimate – with large scatter – the mean density and the redshift of formation as

$$\langle M_{12} \rangle = 40(1 \pm 1), \quad \langle \rho_{vir} \rangle = 2.7 \cdot 10^5 (1 \pm 0.9) M_\odot / kpc^3,$$

$$\langle 1 + z_f \rangle = 3.1(1 \pm 0.3), \quad \langle \Psi(M) \rangle = 0.74 \sigma_8 (1 \pm 0.3)\,, \tag{5.6}$$

and so to partly fill the empty region in Fig. 2 between the galaxies and clusters of galaxies. Main results of our analysis are plotted in Fig. 2 and presented in Table 1.

5.4 The THINGS and LSB galaxies

For 11 LSB and THING galaxies (de Blok et al. 2008; Kuzio de Naray et al. 2008; Chemin et al. 2011) the observed rotation curves are measured up to large distances what allows us to estimate with a reasonable reliability the virial masses M_{vir} and the mean virial density, $\langle \rho_{vir} \rangle$, and, finally, using the relation (2.6) to estimate the redshift of formation and the virial mass of these objects, we get

$$\langle M_{12} \rangle = 0.24(1 \pm 0.8), \quad \langle \rho_{vir} \rangle = 6.2 \cdot 10^5 (1 \pm 0.9) M_\odot / kpc^3,$$

$$\langle 1 + z_f \rangle = 2.7(1 \pm 0.1), \quad \langle \Psi(M) \rangle = 1.6 \sigma_8 (1 \pm 0.2)\,. \tag{5.7}$$

Non the less the complex internal structure of these galaxies and the significant influence of stars, discs and diffuse baryonic component restricts the number of objects for which reasonable DM characteristics can be derived. For 11 galaxies results of our analysis are presented in Table 1 and in Figs. 1 and 2. But even for these galaxies the weak dependence of the measured rotation curves upon their radius demonstrates that the accepted virial mass of galaxies is noticeably underestimated and reliability of obtained results is in question.

5.5 The dSph galaxies

Recently properties of the dSph galaxies were discussed in many papers. Thus, the main observed parameters of 28 dSph galaxies are listed and discussed in Walker et al. 2009 & 2011; Penarrubia et al. 2010; for 13 And galaxies with similar properties results are listed in Collins et al. 2014; Tollerud et al. 2012 & 2014. Extensive list of similar galaxies is also given also by McConnachie 2012. Published characteristics of these galaxies vary from paper to paper and are presented with significant scatter. From samples presented in Walker et al. 2009 & 2011; Collins et al. 201); Tollerud et al. 2012 & 2014 we selected 19 objects with high DM density, what suggests that these objects were formed at high redshifts and can be considered as samples of earlier galaxies responsible for reionization. This means that for these galaxies the redshift of formation z_f should be comparable with redshift of reionization $z_{reio} \sim 9$ determined by WMAP and Planck missions. For other 22 objects of these surveys situation is not so clear and either their published parameters are unreliable or perhaps they were formed later as a surviving companions of more massive objects.

Our sample includes objects in a wide range of masses, what allows us to reveal more reliably the mass dependence of their redshift of formation (Demiański & Doroshkevich 2014). But in this case we have to deal with parameters of DM at the projected half–light radius and they must be recalculated to the virial mass and core parameters, what introduces additional uncertainties. In spite of these problems it is very interesting to compare characteristics of these galaxies with characteristics of clusters of galaxies presented in the previous sections and with theoretical expectations (4.3).

Comparison of the observed circular velocity v_c and velocity dispersion σ_v shows that for the subpopulation of 19 denser objects the half–light radius $r_{1/2}$ corresponds to concentration

$$v_c^2(r)/\sigma_v^2(r) \approx \sqrt{r_{1/2}/r_s} = \sqrt{c_{1/2}}\,,$$

$$\langle c_{1/2}\rangle = \langle r_{1/2}/r_s\rangle \approx 1.6(1 \pm 0.04)\,, \tag{5.8}$$

what allows us to restore the main characteristics of the sample. Thus, the virial mass of the galaxies can be estimated with reasonable precision using (2.2) as

$$M_{vir} = M_s f_m(c) \approx M_s = M_{1//2}/f(c_{1/2})\,,$$

because $0.7 \le f_m(c) \le 1$, for concentrations of interest $3.5 \le c \le 5$. For $c \le 4$ this approach overestimates the virial mass by about 15 - 20%, what is comparable with the precision of measurements. For $4 \le c \le 5$ errors become still smaller. Expression (2.7) can be used to test the internal agreement of such approach. This sample accumulates objects in a wide range of masses $10^6 \le M_{vir}/M_\odot \le 10^9$, that had been formed at high redshifts

$$12.8 \ge 1 + z_f \ge 8.6, \quad \langle 1 + z_f\rangle \approx 9.9(1 \pm 0.1)\,. \tag{5.9}$$

The basic parameters of these objects are found using the function $\Phi(M_{vir})$ (4.6) in (2.6, 4.2, 4.3) what, in contrast with (2.4, 2.5), allows us to reconcile the theoretical expectations (4.2, 4.3) for parameters of the DM dominated halos with the observed ones (6.1). This choice of $\Phi(M_{vir})$ also decreases the redshift of formation of dSph galaxies down to (5.9). Such estimates of z_f are consistent with results of Planck $z_{reio} \sim 9$ (Ade et al. 2016) and are confirmed by estimates of ages of stars $z_f \geq 5-6$ (see, e.g., Weisz et al. 2014; Karachentsev et al. 2015). Large scatter of our estimates is mainly caused by the large scatter of observational parameters. Basic characteristics of these objects are presented in Table 1 and are discussed in section 6.

Using (A.1) for the observed parameters of this survey at the projected half–light radius $r_{1/2}$ we get

$$\langle r_{1/2} \rangle \approx 140pc, \ \langle M_{1/2} \rangle \approx 2.4 \cdot 10^7 M_\odot, \ \langle \theta_{1/2} \rangle \approx 120\,. \tag{5.10}$$

This value of $\langle \theta_{1/2} \rangle$ is larger than (5.2) by a factor of 1.5 . It can be partly caused by our using of the X–ray temperature T_x in (5.2) and velocity dispersion of stars in (5.10).

However this difference can indicate real differences in the internal structures of dSph galaxies and clusters of galaxies that can be induced by different factors that determine the entropy generation in these objects. As was discussed in section 3 for massive clusters of galaxies the entropy of DM component is formed mainly by the violent relaxation of compressed matter, while for dSph galaxies significant contribution comes from initial random motions of matter.

For the ΛCDM spectrum (2.13) and redshift (5.9) we get for the dSph data

$$\langle \Psi(M) \rangle = 1.1\sigma_8(1 \pm 0.08)\,, \tag{5.11}$$

what is quite similar (2.14).

These estimates of $\langle \Psi(M) \rangle$ are by a factor of 2.75 larger than those obtained for the CLASH survey (5.3). This difference suggests the corresponding difference in the amplitude of power spectrum at large and small scales. We will discuss this problem in more details in section 7.1 .

Our results presented in this section depend upon the choice of the function Φ (4.6). To demonstrate the real influence of this factor we reanalyzed the same observational data in the same manner assuming that

$$\Phi(M_{vir}) = 1\,. \tag{5.12}$$

Naturally the observed physical characteristics of objects, $\langle \rho_s \rangle$, $\langle p_s \rangle$, and $\langle S_s \rangle$ remain the same as listed in Table 1 and plotted in Fig. 1 but now differences between expectations (2.5, 4.3) and observations (6.1) become significant. Moreover such choice strongly increases the redshifts of formation and concentrations of halos up to

$$\langle 1 + z_f \rangle \approx 15.7(1 \pm 0.2), \quad \langle \eta_f \rangle \approx 6.5(1 \pm 0.07) \quad \langle c \rangle \approx 11(1 \pm 0.2)\,. \tag{5.13}$$

In turn this immediately changes all self similar parameters and now we get

$$\langle \eta_\rho \rangle \approx 220 M_\odot / kpc^3, \quad \langle \eta_p \rangle \approx 6 \cdot 10^3 eV/cm^3, \quad \langle \eta_s \rangle \approx 0.2 cm^2 eV\,, \tag{5.14}$$

instead of corresponding parameters listed in Table 1 . This growth of z_f decreases estimate (5.11) of the function $\langle \Psi(M) \rangle$ down to

$$\langle \Psi(M) \rangle = 0.73\sigma_8(1 \pm 0.2)\,, \tag{5.15}$$

but as before this estimate significantly exceeds the value (5.3) obtained for the CLASH survey.

Thus the choice $\Phi = 1$ destroys the accordance between expectations (4.3) and observations (6.1) and removes the attractive inference about the self similarity of virialized DM dominated objects in a wide range of masses. On the other hand these values of $\langle z_f \rangle$ and $\langle c \rangle$ (5.13) appear unreliably large. These estimates can be directly tested with more detailed observations even with the already known dSph objects. Non the less the latest observations of PLANCK decreases the redshift of reionization from $z_{rei} \sim 10.5$ (Komatsu et al. 2011) down to $z_{rei} \sim 8.9$ (Ade et al. 2016; Robertson et al. 2015; Mitra et al. 2015), what is quite similar to our estimates (5.9). The physical reason to use the expression (2.6) with the function $\Phi(M_{vir})$ as (4.6) were discussed in sections 2.2 & 3.

5.6 The Kirby catalog of dSph galaxies

Second catalog of dSph galaxies (Kirby et al. 2014) contains 30 satellites of Milky Way and Andromeda with independent measurements of their parameters. Thus some of them significantly differ from those presented in Walker et al. 2009 & 2011 and Tollerud et al. 2012 & 2014. In particular instead of (5.10) we have for this survey at the projected half–light radius $r_{1/2}$

$$\langle r_{1/2} \rangle = 730pc, \quad \langle M_{1/2} \rangle = 10^9\, M_\odot, \quad \langle \theta_{1/2} \rangle = 150\,, \tag{5.16}$$

with significant growth of $\langle r_{1/2} \rangle$ and $\langle M_{1/2} \rangle$. On the other hand, for this sample we get

$$\langle 1 + z_f \rangle = 8.1(1 \pm 0.1), \quad \eta_f \approx 4.1(1 \pm 0.1), \quad \langle \Psi(M_{vir}) \rangle = 1.1\sigma_8(1 \pm 0.1)\,, \tag{5.17}$$

what is quite similar to the previous results (2.14, 5.9, 5.11). Other results for this survey are presented in Table 1 and are plotted in Figs 1 & 2.

This comparison of results obtained for two sets of observations of the same objects allows to verify representativity and reliability of obtained estimates. These data were analyzed in the same manner as the previous ones and the main results are close to those obtained for the previous sample.

5.7 Ultra diffuse galaxies

Now there are new possibilities of observations of the Ultra Diffuse Galaxies (UDG) near M101 (Merrit et al. 2014), in the Virgo cluster (Liu et al. 2015; Beasley et al. 2016), in the Coma cluster (van Dokkum et al. 2015; 2016), and in the Pisces-Perseus supercluster (Martinez-Delgado et al. 2016). For one of this object – DM dominated galaxy Dragonfly 44 (van Dokkum et al. 2016) – there are observations of $M_{1/2}$, $r_{1/2}$, & σ_v what is the same data as for the dSph galaxies. With these data we can repeat the analysis performed in two previous subsections. Thus we get for this galaxy

$$M_{vir} \approx 1.4 \cdot 10^{10} M_\odot, \quad \rho_s \approx 4.2 \cdot 10^8 M_\odot/kpc^3, \quad p_s \approx 7.8eV/cm^3, \quad S_s \approx 0.078 cm^2 keV\,,$$

$$\eta_p = 3.4eV/cm^3, \quad \eta_\rho = 2.4 \cdot 10^7 M_\odot/kpc^3, \quad \eta_s = 3.3 cm^2 keV, \quad c \approx 2.8\,, \tag{5.18}$$

$$1 + z_f \approx 5.2, \quad B^{-1}(\eta_f) \approx 3.8, \quad \eta_f = 3.8, \quad \Psi = 1.1\sigma_8\,.$$

These data are presented in Figs. 1& 2.

As is seen from these Figures this galaxy is located in the halfway between the CLASH clusters and dSph galaxies and quite well fits with other data plotted in these Figures. This can be considered as the independent evidence in favor of our approach and inferences. We hope that further investigations of UDG galaxies will allow to improve our results.

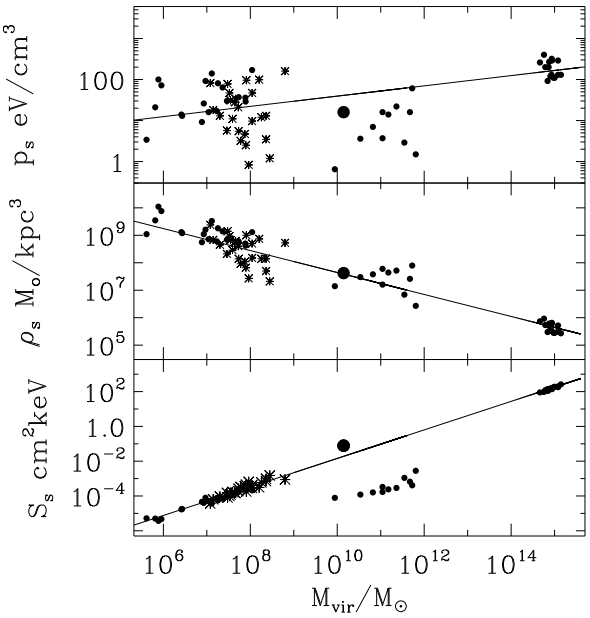

Figure 1. The functions $\langle P_s(M_{vir}\rangle$, $\langle \rho_s(M_{vir}\rangle)$, & $\langle S_s(M_{vir})\rangle$ are plotted for the two sample of dSph galaxies (section 5.5, left points and section 5.6, stars), THING and LSB galaxies (central points) and CLASH clusters of galaxies (right points). For the Dragonfly 44 values (5.18) are plotted by filled dark circle. Fits (6.1) are plotted by solid lines.

5.8 Sample of 8 dSph galaxies

Recently a very detailed discussion of 8 dSph galaxies was performed by Burkert (2015). In this paper application of more complex two component isothermal and King's models are considered. His main results are quite similar to our estimates. It is important that estimates of the central densities exceed our values by a factor ~ 2 what increases the corresponding redshifts z_f by 20 – 30% . Further investigations of dSph galaxies are clearly needed.

6 Cores of DM dominated virialized objects

6.1 Basic characteristics of the DM cores

For two samples of dSph galaxies, Dragonfly 44 galaxy and CLASH clusters of galaxies parameters of their DM cores (the pressure, P_s, density, ρ_s, and entropy, S_s) are plotted in Fig. 1 and are fitted by the expressions:

$$\langle P_s\rangle = 140(1\pm 0.8)eV/cm^3 M_{12}^{0.1}\,,$$

$$\langle \rho_s\rangle = 10^7(1\pm 0.6)\frac{M_\odot}{kpc^3}M_{12}^{-0.45}\,, \tag{6.1}$$

$$\langle S_s\rangle = 0.66(1\pm 0.4)keV\,cm^2 M_{12}^{0.85}\,,$$

$$\langle 1+z_f\rangle = 4.1(1\pm 0.17)M_{12}^{-0.077}\,,$$

where again $M_{12} = M_{vir}/10^{12}M_\odot$. For comparison in Fig. 1 the same functions are also plotted for THING and LSB galaxies. Large deviations of these parameters from the fits

Table 1. Characteristics of DM halos

	CLASH	Groups	Galaxies	dSph	Kirby
N_{obj}	19	30	11	19	30
$\langle M_{12}\rangle$	870	40	$0.2(1\pm0.8)$	10^{-4}	10^{-4}
$\langle\rho_s\rangle$	$5(1\pm0.5)$	$2.7(1\pm0.9)$	$3.4(1\pm0.9)$	$10^5(1\pm0.9)$	$10^5(1\pm0.9)$
$\langle p_s\rangle$	$224(1\pm0.7)$		$0.2(1\pm0.8)$	$10^{-5}(1\pm0.9)$	$10^{-4}(1\pm0.9)$
$\langle T_s\rangle$	$10(1\pm0.3)$		$0.1(1\pm0.5)$	$10^{-3}(1\pm0.8)$	$10^{-3}(1\pm0.8)$
$\langle S_s\rangle$	$1.6(1\pm0.9)$		$0.1(1\pm0.9)$	$10^{-6}(1\pm0.9)$	$10^{-5}(1\pm0.9)$
$\langle c\rangle$	$3.7(1\pm0.2)$			$3.7(1\pm0.2)$	$3.3(1\pm0.2)$
$\langle\Sigma_s\rangle$	$3.4(1\pm0.3)$			$1.0(1\pm0.5)$	$0.8(1\pm0.5)$
$\langle\eta_\rho\rangle$	$16(1\pm0.5)$		$0.6(1\pm0.9)$	$2.2(1\pm0.7)$	$1.5(1\pm0.8)$
$\langle\eta_s\rangle$	$1.2(1\pm0.1)$		$31.(1\pm0.9)$	$0.9(1\pm0.3)$	$1.1(1\pm0.4)$
$\langle\eta_f\rangle$	$3.9(1\pm0.1)$	$3.9(1\pm0.3)$	$2.4(1\pm0.2)$	$4.2(1\pm0.1)$	$4.1(1\pm0.1)$
$\langle 1+z_f\rangle$	$2.3(1\pm0.1)$	$3.1(1\pm0.3)$	$2.3(1\pm0.2)$	$9.9(1\pm0.1)$	$8.1(1\pm0.1)$
$\langle\Psi\rangle/\sigma_8$	$0.4(1\pm0.1)$	$0.7(1\pm0.3)$	$1.6(1\pm0.2)$	$1.1(1\pm0.1)$	$1.1(1\pm0.1)$

Here $\langle M_{12}\rangle = \langle M_{vir}\rangle/10^{12}M_\odot$, $\langle\rho_s\rangle$ & $\langle\eta_\rho\rangle$ are measured in $10^5M_\odot/kpc^3$, $\langle p_s\rangle$ in eV/cm^3, $\langle T_s\rangle$ in keV, $\langle S_s\rangle$ in 10^2cm^2keV, $\langle\Sigma_s\rangle$ in $100M_\odot/pc^2$, $\langle\eta_s\rangle$ in cm^2keV,

are caused by uncertainties in estimates of the influence of baryonic component, of the virial mass and other parameters of the DM cores. Large scatter of the functions (6.1) reflects mainly the large scatter of the observational data and the natural random variations of object characteristics.

Our analysis revealed some unexpected peculiarities in characteristics of cores of the observed DM dominated virialized objects. First is the small variation of parameters η_ρ, η_p, & η_s presented in Table 1 for the five samples of observed virialized objects in a wide range of virial masses. The large scatter of presented results is partly caused by scatter of the observed parameters and by probable influence of neglected factors of evolution such as the impact of baryonic component. This scatter is small for the entropy parameter η_s as the entropy is the more stable characteristic of objects. Moreover for the CLASH sample all parameters of cores are quite close to the expected ones (4.3). We consider this similarity as an evidence in favor of the self similar character of the internal structure of observed DM dominated objects.

Next is a weak variation of the DM pressure in cores of such halos with the virial mass, redshift of formation and other characteristics of these objects. Thus for CLASH and dSph samples the mean virial masses differ by seven orders of magnitude while the central pressures differ by a factor ~ 20 only. In contrast, the entropy of cluster cores significantly – by a factor of $10^6 - 10^7$ exceeds the entropy of DM dominated objects of galactic scale.

Other manifestation of this peculiarity is the weak mass dependence of the surface density of cores (see, e.g., Spano et al., 2008; Donato et al. 2009; Salucci et al. 2011; Demiański & Doroshkevich 2014; Saburova & Del Popolo, 2014; Kormendy & Freeman 2015). For the DM dominated objects in the CLASH sample

$$\langle\Sigma_s\rangle \approx 340(1\pm0.3)\frac{M_\odot}{pc^2}\,, \tag{6.2}$$

and for the objects in dSph sample

$$\langle\Sigma_s\rangle \approx 100(1\pm0.5)\frac{M_\odot}{pc^2}\,.$$

These results are consistent with weak mass dependence of the DM pressure (6.1) as

$$P_s \propto \rho_s M_s / r_s \propto \Sigma_s^2 \,.$$

This shows that (6.2) is a natural result for cores of relaxed DM halos formed from perturbations with the CDM–like power spectrum.

In contrast with (2.5) the quite moderate mass dependence of the observed parameters (6.1, 6.2) confirms the validity of expression (4.6) used for description of DM dominated relaxed halos. Indeed, for the function Φ as defined by (4.6) both expressions (4.5) and (6.1) become very similar to each other and they fit the observational data for the samples with similar scatter. Both expressions for the entropy are almost identical but the expression (6.1) for $\langle P_s \rangle$ more clearly demonstrates weak variations of the DM core pressure with the virial mass of halos. Both of these fits are very preliminary and should be essentially improved with richer observational data with small scatter.

It is important that these basic characteristics of objects depend upon the virial mass only while the earlier used relations (sections 2 & 3) relay on explicit dependence upon the redshift z_f. Thus the relations (4.3) and (6.1) confirm that the redshift z_f is also an explicit function of the virial mass of objects (see also discussion in Demiański and Doroshkevich 2014) what is consistent with the basic ideas of the present day theories of galaxy formation (e.g. Press – Schechter, 1974; Bardeen et al. 1986; Bond et al. 1991; Sheth & Tormen 2002, 2004). Moreover similarity of the power indices in expressions (2.13) and (2.9) confirms the CDM–like shape of the small scale power spectrum.

As well as properties of DM virialized halos discussed in section 3 these inferences have only statistical significance. Non the less allowing for the wide interval of virial masses under consideration, weak variations of the parameters η_ρ, η_p, & η_s introduced in (4.3) and presented in Table 1 demonstrate the self similarity of basic properties of the observed cores of DM dominated galaxies and clusters of galaxies.

Such self similarity naturally appeared in simulations with the simplest power spectrum $p(k) \propto k^n$. For the CDM model simulations show similarity of the dimensionless characteristics of the DM halos such as the NFW density and pressure profiles. On the other hand the regular character of the CDM initial power spectrum (Bardeen et al. 1986) sets up correlations between the virial masses of DM objects and their redshifts of formation. For the observed DM dominated objects the self similarity can be related to the combined influence of the standard violent relaxation and the regular shape of the initial power spectrum of density perturbations. However within the observed objects it is often destroyed by the impact of cooling of the baryonic component.

During previous discussion we used the redshift of object formation, z_f, that is closely correlated with the central DM density and its virial mass. It is important that z_f is clearly linked with the physical process of object formation and in particular with the initial power spectrum. In contrast, the popular use of the observed redshift of clusters of galaxies z_{obs} instead of the z_f for estimates of their virial characteristics is certainly an incorrect procedure. The random character of the redshift $z_{obs} \ll z_f$ is evident for galaxies. For CLASH clusters discussed above this difference is also quite significant,

$$\langle 1 + z_f \rangle \approx 1.7 \langle 1 + z_{obs} \rangle \,.$$

Introduction of z_f instead z_{obs} requires more detailed observations but it decreases artificial variations of cluster characteristics and in particular will change estimates of the redshift evolution of the observed mass function of clusters.

The central pressure and temperature of relaxed objects are determined mainly by the dynamical equilibrium of the compressed, dominating DM component, but as was shown in section 3 the central entropy includes at least two components, namely, the initial entropy of the compressed matter and entropy generated in the course of violent relaxation. Our results indicate that for clusters of galaxies the contribution of the second component dominates. However as was discussed above and is seen from (3.1) and (A.7) for low mass early galaxies the contribution of the initial perturbations can be more important.

6.2 Properties of the baryonic component

Properties of the baryonic component also strongly depend upon the period of object formation. Thus first galaxies such as dSph contain the baryonic component with very low entropy determined by recombination of baryons (see, e.g. Demiański & Doroshkevich 2014). This implies that for these objects the central entropy of the baryonic component is mainly generated in the course of their formation.

For $z_f \leq 10$ the entropy of slightly perturbed intergalactic baryonic component can be partly related to the progressive ionization and heating of the intergalactic gas by the UV background. For redshifts $z_f \leq 3$ when strong photo ionization of HeI and HeII is caused by the hard UV radiation of quasars the temperature and entropy of such baryons can be estimated as

$$T_b \sim 0.7eV(1+z)^{6/7}, \quad S_b \sim 18(1+z)^{-8/7}cm^2keV, \quad z \leq 3\,. \tag{6.3}$$

This entropy strongly exceeds the entropy of the THINGs and LSB galaxies and is similar to the observed entropy of less massive clusters of galaxies. The Jeans mass of such baryonic component increases up to

$$M_J \sim 10^{10} M_\odot (1+z)^{0.2}\,.$$

This shows that for less massive objects formed at $z_f \leq 3$ the baryonic fraction can be sharply suppressed.

At redshifts $z_f \geq 3$ the contribution of quasars to ionizing UV radiation is small and the entropy of intergalactic baryons depends upon the spectrum of softer local UV background. Thus the observed entropy of THING and LSB galaxies is less than (6.3), what indicates that for them the contribution of the initial baryonic entropy is small. This means that probably at redshifts $z_f \geq 3$ the ionization of the intergalactic gas is not accompanied by its essential heating.

7 Shape of the power spectrum

Observations of the relic microwave background radiation allow to determine the shape of the initial power spectrum of density perturbations at large scales starting from clusters of galaxies (Komatsu et al. 2011; Ade et al. 2016). However information about the power spectrum at small scale and composition and properties of dark matter is still missing. In this section we consider in more details the function $\Psi(M_{vir})$ introduced by (2.10) and link its mass variations with the shape of the power spectrum.

7.1 Theory versus observations

Both simulations and observations show that characteristics of the DM dominated halos are much more stable than characteristics of the baryonic component, and they can be used to

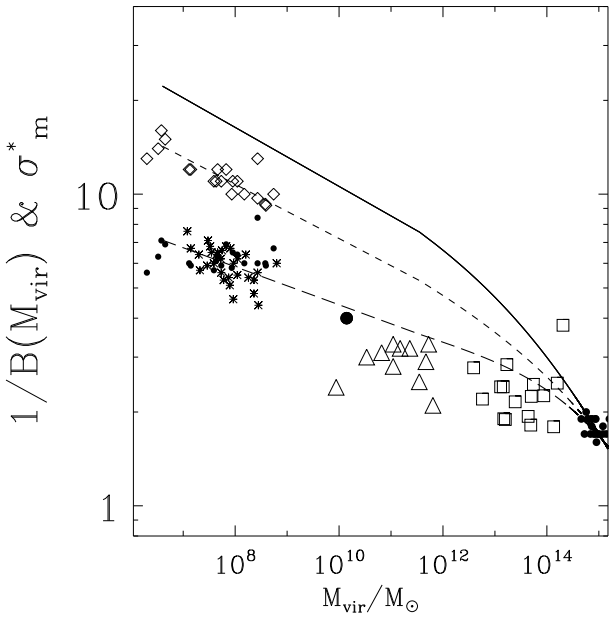

Figure 2. Dispersion of the density perturbations $\sigma_m^* = \sigma_m(M)/0.43$ (2.11, 7.1) for the standard ΛCDM power spectrum (2.13) and the combined spectra (7.3) and (7.4) are plotted by solid, long dashed and dashed lines vs. $M_{vir}/M_\odot$. Function $B^{-1}(M_{vir})$ (1.3) is plotted for the two samples of dSph galaxies (left group of points and stars), for Dragonfly 44 galaxy (filled circle) and for CLASH clusters of galaxies (right group of points). For THINGS and LSB galaxies and for groups of galaxies the functions $B^{-1}(M_{vir})$ are plotted by triangles and squares. For dSph galaxies the function $B^{-1}(M_{vir})$ obtained assuming that $\Phi(M) = 1$ (5.12) is plotted by rhombus.

characterize the small scale power spectrum of density perturbations. Indeed our analysis performed in sections 2, 4 & 5 shows that we can find a one to one correspondence between the observed parameters of the DM halos and the redshift of object formation, z_f. According to the present day models of halo formation (Press, Schechter, 1974; Peebles 1980; Bardeen et al. 1986; Bond et al. 1991; Sheth & Tormen 2002, 2004) the variations of redshift z_f with the virial mass of created objects characterize both the power spectrum of density perturbations and the real period of objects formation. As was discussed in section 2.3 in these models the overdensity that divides the linear and nonlinear periods of the object evolution is a weak function of its virial mass. Therefore we can expect that the function $\Psi(M_{vir})$ describing this division shows also weak dependence upon the virial mass.

However estimates (5.3), (5.6),(5.11), (5.17) and (5.18) demonstrate unexpectedly significant mass dependence of the function $\Psi(M_{vir})$

$$\langle\Psi(M)\rangle/\sigma_8 \approx 0.4,\ 0.74,\ 1.1,\ 1.1,\ 1.1\,.$$

This effect suggests a possible deviation of the small scale power spectrum from that observed at larger scales by the WMAP and Planck missions and now accepted in the ΛCDM cosmological model.

This effect is illustrated in Fig. 2 where the function $B^{-1}(M_{vir})$ (1.3) is plotted for the samples of CLASH clusters, groups of galaxies and for the samples of dSph, UDG, THING and LSB galaxies with both choices of the function $\Phi(M_{vir})$ (4.6, 5.12). These functions are compared with the dispersion of the density perturbations $\sigma_m(M_{vir})$ (2.11) calculated for the

standard ΛCDM power spectrum (2.13). To more clearly represent the trend we plot in Fig. 2 the function

$$\sigma_m^* = \sigma_m(M_{vir})/0.43\,, \tag{7.1}$$

that satisfies the condition

$$\Psi^*(M_{vir}) = \sigma_m^*(M_{vir})B(z_f(M_{vir})) \approx 1\,, \tag{7.2}$$

for the CLASH clusters of galaxies. The strong differences between observations and expectations of the standard CDM–like power spectrum are clearly seen in Fig. 2.

At the same Figure the observed points $B^{-1}(M_{vir})$ are well fitted by functions $\sigma_m^* = \sigma_m/0.43$ obtained for the more complex power spectra

$$p_m(k) = 0.1p_{cdm}(k) + 0.9p_{wdm}(k), \quad \sigma_m^2 = 0.1\sigma_{cdm}^2 + 0.9\sigma_{wdm}^2\,, \tag{7.3}$$

$$p_m(k) = 0.4p_{cdm}(k) + 0.6p_{wdm}(k), \quad \sigma_m^2 = 0.4\sigma_{cdm}^2 + 0.6\sigma_{wdm}^2\,, \tag{7.4}$$

Here $p_{cdm}(k)$ is the standard CDM power spectrum. The function

$$\sigma_{wdm} \approx 1.3\sigma_8/(1 + 0.05M_{12}^{0.4})\,, \tag{7.5}$$

corresponds to a power spectrum describing the contribution of the large scale perturbations only. The three functions $\sigma_m^*(M_{vir})$ plotted in Fig. 2 are identical to each other for $M_{vir} \geq 10^{15}M_\odot$.

As an example of the power spectrum with damped small scale part (7.5) we use the power spectrum of WDM particles (Viel et al. 2005, 2013), namely,

$$p_{wdm}(q) \approx p_{cdm}(q)[1 + (\alpha_w q)^{2.25}]^{-4.46}\,, \tag{7.6}$$

$$q = \frac{k}{\Omega_m h^2}, \quad \alpha_w = 6\cdot 10^{-3}\left(\frac{\Omega_m h^2}{0.12}\right)^{1.4}\left(\frac{1keV}{m_w}\right)^{1.1}\,,$$

where $m_w \sim (50-100)eV$ and the comoving wave number k is measured in Mpc^{-1}. This value m_w corresponds to the damping scales M_{dmp} and D_{dmp}

$$\sigma_{wdm}(M_{dmp}) = 0.5\sigma_{wdm}(0), \quad M_{dmp} = 1.8\cdot 10^{15}M_\odot\,. \tag{7.7}$$

$$D_{dmp} \sim (10-20)h^{-1}Mpc\,.$$

Let us note however that in p_{wdm} and σ_{wdm} the mass m_w is only a formal parameter allowing to introduce the suitable damping scales M_{dmp} and D_{dmp} in the function σ_{wdm} (7.5) and such particles need not really exist. The function σ_{wdm} (7.5) is weakly sensitive to the shape of the spectrum (7.6), when the suppression of power occurs sufficiently rapidly. For example, the spectrum with the Gaussian damping

$$p_{wdm}(q) \approx p_{cdm}(q)[1 + \exp(q^2/q_{dmp}^2)]^{-2}\,, \tag{7.8}$$

and a suitable value q_{dmp} provides the same σ_{wdm} (7.5). At the same time the CDM–like shape of the small scale power spectrum is preserved in (7.3), (7.4) what is consistent

with similarity of the expressions (2.13) and (2.9) for $M_{12} \leq 1$. It is apparent that such decrease of the amplitude of small scale perturbations eliminates discrepancy between estimates (2.14, 5.3, 5.6 & 5.11) of the function $\Psi(M_{vir})$.

The difference between the power spectra (7.3) and (7.4) is caused by the choice of the function $\Phi(M_{vir})$. But as is seen from Fig. 2 and from comparison of (5.3) and (5.15) even for the case (7.4) the differences between the observed values $B^{-1}(M_{vir})$ and σ_{cdm} for the ΛCDM power spectrum remain quite large. These results show that in contrast with some theoretical expectations (see, e.g. Ellis et al. 2016) the power spectrum at small scales should be significantly suppressed as compared with the standard ΛCDM model but without changing its shape.

Of course these results cannot be considered as a strong indication that the standard ΛCDM model should be modified but they demonstrate again some intrinsic problems of this model. The strong links of DM characteristics of observed relaxed objects with the initial power spectrum and cosmological model is well known. Results presented in Figs. 1 and 2 demonstrate the regular correlations of properties of DM component with the virial masses of the relaxed objects. These correlations can be successfully interpreted in the framework of the standard model of halo formation based on the excursion set approach but applied for the more complex power spectrum. However these unexpected results should be tested with suitable set of high resolution simulations before their real status will be accepted.

Of course the observational base used in our discussion is very limited and it should be extended by more observations of objects with masses $M \leq 10^{12} M_{\odot}$, what may be crucial for determination of the shape of the initial power spectrum, the real composition of dark matter and even the models of inflation. Unfortunately more or less reliable estimates of the redshift z_f can be obtained mainly for the DM dominated objects or for objects with clearly discriminated impact of DM and baryonic components. Here we use results obtained for 11 THINGS and LSB galaxies (de Blok et al. 2008; Kuzio de Naray et al. 2008) but even for them both the virial masses and redshift z_f are strongly underestimated. The most promising results can be obtained for the mentioned in section 5.7 population of Ultra Diffuse Galaxies now represented by the galaxy Dragonfly 44 only (see Figs 1 & 2). We hope that the list of possible appropriate candidates will be extended.

Next important problem is the reliability of the approach used in our analysis and obtained results. It depends upon the representativity of the observational data and is moderate because of the very limited available data and their significant scatter. Progress achieved during last years makes it possible to begin discussion of this problem but the available data allow only qualitative character of such discussion. Indeed, the problem of estimates of the mass, density and other parameters of the observed objects is quite complex, methods used for such estimates are very rough and model dependent and their reliability is limited. Moreover the influence of the baryonic component increases scatter of the measured parameters and makes it difficult to estimate the real precision of our results. However we hope that because of the high importance of this problem such observations will be extended and their precision improved.

7.2 'Too Big To Fail' approach

Essential support for our inferences comes from comparison of the circular velocities of simulated low mass galaxies and the observed dSph satellites of Milky Way and Andromeda (Boylan–Kolchin et al. 2012; Garrison–Kimmel et al., 2014a,b; Tollerud et al. 2014; Hellwing et al. 2015; Brook, & Cintio 2015). It demonstrates that the circular velocities of

objects in simulations performed with the standard ΛCDM power spectrum reproduce observations for more massive objects but regularly overestimate the observed circular velocities for less massive objects.

It seems that this discrepancies can be related to efficiency of the environmental processes and complex evolutionary history in the context of the hierarchical formation of objects. This problem is discussed by Wetzel et al. 2015. But the similar effects are observed also for galaxies in the Local Group, where in particular there is the deficit of low mass galaxies in observations as compared with predictions of the standard simulations (Klypin et al. 2015). These discrepancies are smaller for simulations performed with suppressed power at small scale (Garrison–Kimmel et al., 2014b; Marsh & Silk 2014). However as was noted above simulations with the standard WDM power spectrum cannot reproduce observations.

These results show that more complex improvements of the standard theoretical models are required. But these indications of qualitative disagreements between standard simulations and observations are not followed by quantitative estimates of required corrections.

7.3 Extended ΛCDM model.

The important result of our analysis is the indication of a weakness of the standard ΛCDM cosmological model and great potential of models with more complex shape of the power spectrum. However our approach indicates that the basic element of such modified power spectrum could be the large contribution ($\sim 70\%$) of the spectrum often associated with particles with large damping scale (7.7). Non the less such partial damping of the power spectrum does not forbid formation of less massive objects but rather decreases their rate of formation relatively to the standard ΛCDM – like power spectrum. It is noteworthy that after 30 years of absolute domination of the CDM model we begin to consider more complex versions of the HDM models (Doroshkevich et al. 1980a,b).

It is important that the observed characteristics of objects can be described by the linear combination of power spectra and so by the damping scales that in turn depend both upon particle masses and velocities. This means that the construction of an adequate complex cosmological model should start with complex inflation models or/and include discussion of DM composition with estimates of the actual damping scales and transfer functions allowing also for linear evolution of perturbations at $z \leq z_{eq}$.

For the models with one component DM the assumption of the more complex primeval power spectrum is required, what implies more complex inflation models (or some other equivalent assumption). However in this case the condition $\Psi(M) \approx const.$ (2.12) is carried out at $z \leq z_{eq}$ and expressions (7.3) – (7.7) correctly describe the sequential process of objects formation. In contrast, for the more interesting models with multi component composition of DM this description should be corrected. As is shown in Appendix B in such models the complex evolution of perturbations leads to deformation of the transfer function even at small redshifts and to the redshift dependence of the function $\Psi(M, z)$ (2.10). In turn this complicates the description of the sequential object formation. For such models our estimates (7.3) – (7.7) become qualitative and approximate. They should be improved by comparison with suitable simulations.

It seems that the simplest such model is a suitable combination of very massive and light particles what leads to a complex shape of the transfer function after the period of recombination (see, e.g. discussion in Boyarsky et al. 2009a,b). However abilities of this simple model are strongly restricted by the period of cosmic nucleosynthesis. In the standard

model with the three oscillating neutrinos the effective number of light particles is

$$N_{eff} = 3.046\,,$$

(Mangano et al. 2006) and the small difference between this value and latest estimates (Ade et al. 2016) makes theoretical models more complex. Thus for discussions of the sterile neutrinos with mass $m \sim 1eV$ it is necessary to assume that they cannot be in thermal equilibrium before the period of cosmic nucleosynthesis (see, e.g., Abazajian 2012, 2015; Kopp et al., 2013; Zysina, Fomichev & Khruschov 2014). Recently restrictions on the properties of sterile neutrinos were placed by the Ice Cube observations (Aartsen et al. 2016).

Of course all these inferences are very preliminary. Thus, here we use the power spectra with the transfer function (7.6) or with Gaussian damping (7.8). More refined description of the power spectrum and specially further progress in the observations of DM dominated objects with suitable virial masses will improve the best model parameters and estimates of the masses and composition of the DM particles. Non the less even today replacement of some fraction of CDM particles by particles with $m_w \sim 3-10\,keV$ can be considered. Modification of the spectrum by such particles, identified now (according to majority preference) as the sterile neutrinos can be included in (7.3) as a third component without noticeable changes of Fig. 2. Indeed, the available sample of the observed DM dominated objects does not yet allow to make any far–reaching conclusions about the actual properties of DM particles.

The widely discussed controversial characteristics of DM objects such as the core–cusp problem, or number of low mass satellites (see, e.g., Bovill & Ricotti, 2009; Koposov et al., 2009; Walker, & Penarrubia, 2011; Boylan-Kolchin et al., 2012; Penarrubia et al. 2012; Governato et al. 2012; Sawala, 2013; Teyssier et al. 2013; Laporte et al. 2013; Collins et al. 2014; Miller et al. 2014) depend upon the dissipative scale and the shape of the power spectrum. This fact supports the hope that these problems also can be successfully resolved in the framework of more complex cosmological models (see, e.g., Pilipenko et al. 2012).

Accurate simulations with various power spectra and/or DM composition are required before we will have next generation of cosmological models with more reliable properties of the DM component. These expectations are supported by moderate results of the first published simulations of the clearly artificial WDM cosmological models (Maccio 2012, 2013; Angulo, Hahn, Abel, 2013; Schneider, Smith & Reed, 2013; Wang et al. 2013; Libeskind et al. 2013; Marcovič & Viel 2013; Schultz et al. 2014; Schneider et al. 2014; Dutton et al. 2014).

8 Conclusions

In this paper we propose a new approach that could solve some important problems of modern cosmology:

1. Explain the self similarity of the internal structure of virialized DM dominated objects in a wide range of masses, what is manifested as the regular dependence of the central pressure, density, entropy and the epoch of halos formation (4.3, 6.1) upon the virial mass of objects.

2. Unexpectedly weak dependence of the DM pressure and surface density of cores of DM dominated virialized objects on their virial masses.

3. Establish the real composition of the dark matter and the shape of the small scale power spectrum of density perturbations .

Summing up let us note that the proposed approach allows us to consider and to compare properties of the observed DM dominated objects in an unprecedentedly wide range of masses $10^6 \leq M_{vir}/M_\odot \leq 10^{15}$. Main results presented in Table 1 and plotted in Fig. 1 unexpectedly favor the regular self similar character of the internal structure of these objects, what confirms the main expectations of the NFW model and the regular character of the power spectrum without strong peaks and deep troughs.

On the other hand as is seen from Fig. 2 our results favor the models with more complex power spectrum with significant excess of power at cluster scale and/or, alternatively, deficit of power at dwarf galactic scales. Both alternatives seem to be quite important and call for more detailed observational study of DM dominated objects. Our results supplement the traditional investigations of galaxies at high redshifts (McLeod et al. 2015; Robertson et al. 2015; Bouwens et al., 2015a,b; Ellis et al. 2016).

Here we consider a phenomenological model of the power spectrum that is composed of fraction $g_{cdm} \sim 0.1 - 0.4$ of the standard CDM spectrum and fraction $g_{wdm} \sim 0.9 - 0.6$ of the HDM spectrum with the transfer function (7.6). Unexpectedly in the spectrum (7.3) the contribution of low mass particles with relatively large damping scale (7.7) dominates, what can be considered as reincarnation in a new version of the earlier rejected HDM model. Further progress can be achieved with more complex models of the power spectrum and/or more realistic transfer functions instead of (7.6, 7.8), what implies also more realistic complex composition of the DM component (such as some sterile neutrino models). In particular it is possible to discuss an excess of power localized at small scale. In some respect such an excess of power reminds the isocurvature models (see, e.g. Savelainen et al. 2013) with similar predictions and problems. However all such problematic multi parametric proposals should be considered in the context of the general cosmological and inflationary models.

The approach used in this paper for discussion of composition and properties of the DM particles is very indirect. We consider effects of strongly nonlinear multistep evolution of perturbations resulting in observed properties of the relaxed objects. The nonlinear evolution usually leads to a strong loss of information about the primeval perturbations and composition of the DM component. These losses are further enhanced by the masking effects of dissipative evolution of the baryonic matter. To reveal the missing impact of the DM composition and primeval perturbations we discuss the most conservative characteristics of the observed DM dominated objects by comparing these data with numerical simulations majority of which are now focused on studying evolution of the standard ΛCDM model.

We believe that more detailed conclusions will be made on the basis of special simulations and after accumulation of more representative observational sample of high precision measurements of properties of DM dominated objects.

8.1 Acknowledgments

This paper was supported in part by the grant of the President of RF for support of scientific schools NSh-6595.2016.2. We thank S. Pilipenko, A. Klypin, B. Komberg, A. Saburova, M Sharina and R. Ruffini for useful comments. Our analysis would not be possible without detailed measurements presented in cited papers. We thanks the referee for constructive comments that significantly improved the text and eliminated many unclear statements.

A Entropy of the relaxed DM halos

Here we estimate the two main components of entropy of DM relaxed halos. First is the entropy generated during compression and violent relaxation of a spherical DM cloud at rest (Peebles 1967; 1980). The other one includes entropy generated by random motions associated with initial density perturbations.

A.1 The mean entropy of halos: Peebles model

In this model the evolution and relaxation of DM halos with zero initial entropy is considered. Thus this model demonstrates that some entropy is really generated within collapsed and relaxed DM halos even without any initial entropy. To obtain rough estimate of this entropy we use the well known correlations between the gravitational U and internal W energy of virialized object,

$$\theta_{vir} = \frac{U}{W} \approx \frac{GM_{vir}}{R_{vir}T_x} = const\,,$$

where T_x is the halo temperature and the value of the *const* depends on the internal structure of the object. Thus for 180 observed clusters of galaxies with masses $10^{13} \le M_{vir}/M_\odot \le 10^{15}$ we have

$$\theta_{vir} = \frac{M_{vir}}{10^{12}M_\odot}\frac{1Mpc}{R_{vir}}\frac{1kev}{T_x} \approx 72(1 \pm 0.08)\,. \tag{A.1}$$

Using this relation and the estimates of the mean density of relaxed DM halos (2.6) we get

$$R_{vir} \approx \frac{0.33MpcM_{12}^{1/3}}{(1+z_f)\Phi^{1/3}}, \quad T_x \approx 0.04M_{12}^{2/3}(1+z_f)\frac{72\Phi^{1/3}}{\theta_{vir}}keV\,,$$

$$\langle S_{vir}\rangle \approx \frac{T_x}{\langle n_{DM}\rangle^{2/3}} \approx 10^{-2}\frac{M_{12}^{2/3}\mu_{DM}^{2/3}}{(1+z_f)\Phi^{1/3}}\frac{72}{\theta_{vir}}cm^2keV\,, \tag{A.2}$$

$$\mu_{DM} = m_{DM}/m_b\,.$$

Here n_{DM} is the mean number density of DM particles in the halo, m_{DM} and m_b are the masses of DM particles and baryons. Using the relation (2.9) we get

$$\langle S_{vir}(M)\rangle \approx 4.3M_{12}^{0.74}cm^2keV\frac{\mu_{DM}^{2/3}}{\Phi^{1/3}}\frac{\eta_f}{4.1}\frac{72}{\theta_{vir}}\,, \tag{A.3}$$

what is comparable with observational estimates (6.1). However these estimates apply mainly to peripheries of halos with large entropy.

A.2 The entropy of halos: contribution of random motions

According to the Zel'dovich approximation and in accordance with simulations based on the ΛCDM cosmological model the velocity dispersion along any principle direction is (see, e.g., Demiański et al. 2011)

$$\sigma_U = \frac{H(z)}{1+z}\beta(z)B(z)\frac{\sigma_s}{\sqrt{3}} \approx \frac{350km/s}{\sqrt{1+z}}\frac{\sigma_8}{0.8}\Theta_m^{-1}\,, \tag{A.4}$$

where the functions $H(z)\,\&\,B(z)$ were introduced in (1.1),

$$\sigma_s^2 = \frac{1}{2\pi}\int_0^\infty p(k)dk, \quad \beta(z) = -\frac{1+z}{B(z)}\frac{dB(z)}{dz}\,,$$

$$\sigma_s \approx 9.3h^{-1}Mpc\Theta_m^{-1}\sigma_8/0.8\,.$$

However all actual velocities within the compressed clouds do not exceed 50 - 100 km/s because the velocity (A.4) is dominated by the random velocity of the halo as a whole. To obtain a rough estimate of random motions of particles accumulated within the compressed halo we can use the relation

$$\sigma_v^2(M_{vir}, M_c) = \frac{1}{2\pi\sigma_s^2}\int_0^\infty dk\, p(k)\Xi(k, M_{vir}, M_c)\,, \tag{A.5}$$

$$\Xi(k, M_{vir}, M_c) = 1 + W^2(k, M_{vir}) - 2W(k, M_{vir})W(k, M_c)\,,$$

where the function $W(k, M)$ was introduced in (2.11), M_{vir} is the virial mass of a halo and $M_c \leq M_{vir}$ is the mass of the central core of this halo. The function $\sigma_v^2(M_{vir}, M_c)$ rapidly increases with the virial mass M_{vir} but only weakly depends upon the mass M_c. For $M_c = 0$ it is well fitted by the expression

$$\sigma_v^2(x) = 1.5\cdot 10^{-2}x^{0.6}/(1 + 0.2x^{0.35})\,. \tag{A.6}$$

Using these results we can roughly estimate the temperature T_{rnd} and the entropy $S_{rnd}(M_{vir})$ of the compressed matter within a halo with a mass M_{vir} formed at the redshift z_f as

$$T_r(M_{vir}) \approx \frac{3m_{DM}\sigma_U^2}{2}g_r\sigma_v^2(M_{vir}) \approx \frac{30M_{12}^{0.6}\mu_{DM}}{1+z_f}g_r eV\,,$$

$$S_r = \frac{T_r m_{DM}^{2/3}}{\langle\rho_m\rangle^{2/3}}g_r \approx 220cm^2keV\frac{M_{12}^{0.6}g_r}{(1+z_f)^3}\mu_{DM}^{5/3}\,, \tag{A.7}$$

where g_r is a random factor that determines the fraction of energy of random motions (A.5) accumulated by the halo. Using the correlation between the redshift z_f and the virial mass of halo (2.9) we get

$$S_r(M_{vir}) \approx 6.4M_{12}^{0.81}\mu^{5/3}g_r(\eta_f/4.1)^3cm^2keV\,, \tag{A.8}$$

what is comparable with observational estimates (6.1). It seems that this channel of entropy generation is more important for less massive halos.

A.2.1 The entropy of intergalactic gas

After reionization the intergalactic gas is heated by the UV radiation and its temperature T_b is close to 10^4K with high spatial variations determined by the inhomogeneities of the UV foreground. The entropy of this gas can be estimated as

$$\langle S_{bar}\rangle \approx \frac{\langle T_b\rangle}{\langle n_b\rangle^{2/3}} \approx \frac{4cm^2keV}{(1+z_f)^2} \sim 0.16M_{12}^{0.15}cm^2keV\,. \tag{A.9}$$

B Evolution of perturbations in two component non relativistic medium

The evolution of perturbations in two component non relativistic medium were considered by Grishchuk & Zel'dovich 1981. Let us assume that the first component is composed of light nonrelativistic particles with density $\rho_1 = \alpha_1\langle\rho(z)\rangle \propto (1+z)^{-3}$, the pressure $p_1 \propto \rho_1^{5/3}$ and the sound speed $\beta_1 \propto 1+z$. The second component is composed of massive particles with density $\rho_2 = \alpha_2\langle\rho(z)\rangle \propto (1+z)^{-3}$, $\alpha_2 = 1-\alpha_1$ and negligible pressure and sound speed, $p_2 = 0$, $\beta_2 = 0$. In this case the evolution of the density perturbations is described by the equations

$$y^2\delta_1'' + \frac{y}{2}\delta_1' - \frac{3}{2}[\alpha_1\delta_1 + \alpha_2\delta_2 - \kappa^2 y^2\delta_1] = 0 \tag{B.1}$$

$$y^2\delta_2'' + \frac{y}{2}\delta_2' - \frac{3}{2}[\alpha_1\delta_1 + \alpha_2\delta_2] = 0$$

where $'$ denotes derivative with respect to the redshift $y = 1+z$, $\delta_1 = \delta\rho_1/\rho_1$, $\delta_2 = \delta\rho_2/\rho_2$, are density perturbations in components 1 & 2, $\kappa^2 = \beta_1^2 k^2$ and k is the comoving wave number.

For large scales ($\kappa \to 0$) we get the usual result for the increasing (c_1) and decreasing (c_2) adiabatic modes

$$\alpha_1\delta_1 + \alpha_2\delta_2 \approx c_1(1+z)^{-1} + c_2(1+z)^{3/2}\,, \tag{B.2}$$

and for two entropic modes we get

$$\delta_1 - \delta_2 \approx c_3 + c_4(1+z)^{-1/2}\,. \tag{B.3}$$

On the other hand for the small scale perturbations with $\alpha_1\delta_1 \ll \alpha_2\delta_2 \ll \kappa^2 y^2\alpha_1\delta_1$ we get

$$\delta_2 \approx c_5(1+z)^{-\gamma}, \quad \gamma = (\sqrt{1+24\alpha_2} - 1)/4\,, \tag{B.4}$$

$$\delta_1 \approx c_6(1+z)^{1/4}J_{1/4}[\kappa(1+z)] \propto (1+z)^{-1/4}$$

where J_ν is the Bessel function. For $\alpha_2 = 1$ we get from (B.4) again that $\delta_2 \propto (1+z)^{-1}$, but $\gamma \leq 1$ for $\alpha_2 \leq 1$.

These results demonstrate that for the two component medium with strongly different masses of particles the spectrum of perturbations is distorted. Thus if for large scale perturbations the amplitude grows as $\delta_{1,2} \propto (1+z)^{-1}$, then for small scale perturbations we get even for heavy particles $\delta_2 \propto (1+z)^{-\gamma}$ (B.4) with $\gamma \leq 1$. For the critical value $\alpha_2 = 1/8$ we get $\gamma = 1/4$, that is the same as the exponent for the small scale perturbations of the other component described by δ_1. Thus in this case perturbations in both media evolve in the same way.

References

[1] Aartsen et al. 2016, Phys. Rev.Lett. 117, 071801

[2] Abazajian, K., Acero, M., Agarwalla, S., et al., 2012, arXiv:1204.5379

[3] Abazajian, K., Arnold, K., Austerman, J., et al, 2015, Aph, 63, 66

[4] Abbott, T., Abdalla, F., Allam, S., et al. 2015, arXiv:1507.05552

[5] Abdallah, J., Araujo, H., Arbey, A., et al., 2015, PDU, 9, 8

[6] Adam, R., Comis, B., Macias-Perez, J., et al., 2015, A&A, 576, 12

[7] Ade, P., Aghanim, N., Arnaud, M., et al. 2016, A&A, 594, 13

[8] Agnese, R., Anderson, A., Asai, M., et al. 2014, PhRvL, 112x1302

[9] Angloher, G., et al., 2013, Eur.Phys.J., C72, 1971

[10] Anderhalden, D., Schneider, A., Maccio, A., Diemand, J., Bdertone, G., 2013, LCAP, 03, 014

[11] Angulo, R., Hahn, O., Abel, T., 2013, MNRAS, 434, 3337

[12] Arnaud, M., Pointecouteau, E., Pratt, G., 2005, A&A, 441, 893

[13] Arnaud, M., Pratt, G., Piffaretti, R. et al., 2010, A&A, 517, 92;

[14] Balazs, L., Bagoly, Z., Hakkila, J. et al. 2015, MNRAS, 452, 2236

[15] Bardeen J.M., Bond J.R., Kaiser N., & Szalay A., 1986, ApJ, 304, 15

[16] Baring, M., Ghosh, T., Queiroz, F., Sinha, K., 2016, PhRvD, 93.103009;

[17] Battaglia, N., Bond, R., Pfrommer, C., Sievers, J., 2015, ApJ, 806, 43

[18] Battye, R., Moss, A., 2014, PhRvL., 112e1303

[19] Battye, R., Charnock, T., Moss, A., 2015, PhRvD..91j3508

[20] Bennet C., et al., 2003, ApJS,, 148, 1

[21] Beasley, M., Romanowsky, A., Pota, V., et al., 2016, ApJ, 819, L20

[22] Berezhiani, Z., Dolgov, A., Tkachev, I., 2016, PhRvD, 92f1303;

[23] Berezinsky, V., Dokuchaev V., Eroshenko Yu., 2014, Phys. Usp. 57, 1

[24] Bernabei, R., Belli, P., Capella, F., et al., 2010, Eur.Phys.J., C67, 39

[25] Bhattacharya, S., Habib, S., Heitmann, K., Vikhlinin, A., 2013, ApJ, 766, 32

[26] Blennow, M., Ccoloma, P., Fernandez–Martinez, E., Machado, P., Zaldivar, B., 2016, JCAP, 04, 015

[27] Blinnikov, S., 2014, Phys. Usp. 57 183

[28] Bond, R., Cole, S., Efstathiou, G., Kaiser, N., 1991, ApJ, 379, 440

[29] Borsanyi, S., Dierigl, M., Fodor, Z., et al., 2016, PhLB, 752, 175

[30] Bovill, M, Ricotti, M., 2009, ApJ, 693, 1859

[31] Bouwens, R., Illingworth, G., Oesch, P. et al.,, 2015a, ApJ, 811, 140

[32] Bouwens, R., Oesch, P., Labbe, I., et al., 2015b, arXiv:1506.01035

[33] Boyarsky, A., Lesgourgues, J., Ruchayskiy, O., Viel, M., 2009a, JCAP, 05, 012

[34] Boyarsky, A., Lesgourgues, J., Ruchayskiy, O., Viel, M., 2009b, PhRvL, 102t1304

[35] Boyarsky, A., Ruchayskiy, O., Shaposhnikov, M., 2009c, ARNPS, 59, 191

[36] Boylan-Kolchin, M., Bullok, J., Kaplinghat, M., 2012, MNRAS, 422, 1203

[37] Branchesi, M., Gioia, I., Fanti, C.,Fanti, R., 2007, A&A, 472, 739

[38] Breddels M., & Helmi, A., 2014, ApJ, 7911, 3

[39] Brook, C., Di Cintio, A., Knebe, A., Gottlber, S.; Hoffman, Y., Yepes, G., Garrison-Kimmel, S., 2014, ApJ., 784, L14

[40] Brook, C., Cintio, A., 2015, MNRAS, 450, 3920

[41] Brooks, A., & Zolotov, A., 2014, ApJ, 786, 87

[42] Bryan, G., Norman, M., 1998, ApJ, 495, 80

[43] Bulbul, E., Markevitch, M., Foster, A., Smith, R., Loewenstein, M., Randall, S., 2014, ApJ, 789, 13

[44] Bullock, J., Kolatt, T., Sigad, Y. et al., 2001, MNRAS, 321, 559

[45] Burenin, R., Vikhlinin, A., 2012, Astronomy Lett., 38, 1

[46] Burkert A., 1995, ApJ, 447, L25

[47] Burkert A., 2015, ApJ, 80, 158

[48] Chemin, L., de Blok, W., Mamon, G., 2011, AJ, 142, 109

[49] Collins, M., Chapman, S., Rich, R., et al., 2014, ApJ, 783, 7

[50] Croston, J., Pratt, G., Bohringer, H., et al., 2008, A&A, 487, 431

[51] de Blok, W., Walter, F., Brinks, E., Trachternach, C., Oh, S.-H., Kennikutt, R., 2008, AJ, 136, 2648

[52] Demiański, M., Doroshkevich, A., 1999, ApJ, 512, 527

[53] Demiański, M., Doroshkevich, A., 2004, A&A, 422, 423

[54] Demiański, M., Doroshkevich A., 2007, PhRvD.,7513517

[55] Demiański, M., Doroshkevich, A., Pilipenko, S., Gottlöber, S., 2011, MNRAS, 414, 1813.

[56] Demiański, M., Doroshkevich A., 2014, MNRAS, 439, 179.

[57] Diemand, J., Kuhlen, M., Madau, P., 2007, ApJ, 667, 859

[58] Diemer, B., More, S., Kravtsov, A., 2013, ApJ, 766, 25

[59] Diemer, B., Kravtsov, A., 2014, ApJ, 789, 1

[60] Doroshkevich, A., Khlopov, M., Sunyaev, R., Zel'dovich, Ya., 1980a, SvAL, 6, 252

[61] Doroshkevich, A., Khlopov, M., Sunyaev, R., Szalay, A., Zel'dovich, Ya., 1980b, Proc. 10th Texas Symposium on Relativistic Astrophysics, Ann.New York Acad. Sci., 375, 32.

[62] Doroshkevich A., Zel'dovich Ya., 1981, JETP, 80, 801

[63] Doroshkevich, A., Khlopov, M., 1984, MNRAS, 211, 277.

[64] Doroshkevich, A., Khlopov, M., Kotok, E., 1986, SvA., 30, 251

[65] Doroshkevich, A., Klypin, A., Khlopov, M., 1988, SvA., 32, 127

[66] Doroshkevich A., Verkhodanov, O., 2011, PhRvD, 83d3002

[67] Doroshkevich A., Lukash, V., Mikheeva, E., 2012, PhyU., 55, 3

[68] Dutton, A., Maccio, A., 2014, MNRAS, 441, 3359

[69] Einasto, M., 2014, arXiv:1409.1347

[70] Eisenstein, D., Hu, W., 1998, ApJ., 496, 605

[71] Ellis, J., Garcia, M., Nanopulos, D., Olive, K., 2016, CQGra, 33i4001;

[72] Enqvist, K., Nadathur, S., Sekiguchi, T., Takahashi, T., JCAP, 09, 067

[73] Essig, R., Jaros, J., Wester, W., et al., 2013, arXiv:1311.0029

[74] Feng, J., 2010, ARA&A, 48, 495

[75] Ferrer, F., Hunter, D., 2013, JCAP, 09, 005

[76] Fillmore J.A., & Goldreich P., 1984, ApJ, 281, 1

[77] Garrison-Kimmel, S., Boylan-Kolchin, M., Bullock, J., Kirby, E., 2014a, MNRAS, 444, 222

[78] Garrison-Kimmel, S., Horiuchi, S., Abazajian, K., Bullock, J., Kaplinghat, M., 2014b, MNRAS, 444, 961

[79] Gorbunov, D., 2014, Phys. Usp. 57 503

[80] Governato, F., Zolotov, A., Pontzen, A., et al., 2012, MNRAS, 422, 1231

[81] Grishchuk, L., & Zel'dovich, Ya., 1981, Astron. Zh., 56, 472

[82] Gurevich, A., Zybin, K., 1995, Phys.Usp., 38, 687

[83] Hellwing, W., Frenk, C., Cautun, M., et al. 2016, MNRAS, 457, 3492

[84] Hinshaw G., Larson, D., Weiland, J., et al., 2013, ApJS, 208, 19

[85] Horiuchi, S., Bozek, B., Abazajian, K., Boylan-Kolchin, M., Bullock, J., Garrison-Kimmel, S., Onorbe, J., 2016, MNRAS, 456, 4346

[86] Horvath, I., Bagoly, Z., Hakkila, J., Toh, L., A&A, 584, 48

[87] Karachentsev, I.Makarova, L., ,Makarov, D., Tully, R., Rizzi, L., 2015, MNRAS, 337, L85

[88] Khedekar, S., Churazov, E., Kravtsov, A. et al., 2013, MNRAS, 431, 954

[89] Kirby, E., Bullock, J., Boylan-Kolchin, M., Kaplinghat, M., Cohen, J., 2014, MNRAS, 439, 101

[90] Klypin, A. Kravtsov, A., Valenzuela. O., Prada, F., 1999, ApJ, 522, 82

[91] Klypin, A. Karachentsev, I., Makarov, D., Nasonova, O., 2015, MNRAS, 454, 1798

[92] Klypin, A. Trujillo-Gomez, S., Primack, J., 2011, ApJ, 740, 102;

[93] Komatsu, E., et al. 2011, ApJS, 192, 18

[94] Koposov, S., Yoo, J., Rix, H.W., Weinberg, D., Maccio, A., Escude, J., 2009, ApJ, 696, 2179

[95] Kopp, J., Machado, P., Maltoni, M., Schwetz, T., 2013, JHEP, 05, 050

[96] Kormendy, J., & Freeman, K., 2015, IAUS, 311, 72,

[97] Kravtsov, A., Borgani, S., 2012, ARA&A, 50, 353

[98] Kusenko, A., Phys.Rep.,2009, 481, 1

[99] Kuzio de Naray, R., Mcgaugh, S., de Blok, W., 2008, ApJ, 676, 920

[100] Lacey, C., & Cole, S., 1993, MNRAS, 262, 627

[101] Laporte, C.,. Walker, M., Penarrubia, J., 2013, MNRAS, 433, 54L

[102] Larson, D.., et al. 2011, ApJS, 192, 16

[103] Libeskind, N., Di Cintio, A., Knebe, A., et al., 2013, PASA, 30, 39

[104] Lithwick Y., Dalal N., 2011, ApJ, 734, 100L

[105] Liu, C., Peng, E., Cote, P., et al., 2015, ApJ, 812, L34

[106] Lloyd–Davies, E., 2011, MNRAS, 418, 14

[107] Ludlow, A. Navarro, J., Boylan-Kolchin, M., et al., 2013, MNRAS, 432, 1103L

[108] Ludlow, A. Bose, S., Angulo, R., et al. 2016, MNRAS, 460, 1214

[109] Maccio, A., Paduroiu, S., Anderhalden, D., Schneider, A., Moor, B., 2012, MNRAS, 424, 1105

[110] Maccio A., Ruchayskiy O., Boyarsky A., Munos–Cuartas J., 2013, MNRAS, 428, 882

[111] Makarov, D., Karachentsev, I., 2011, MNRAS, 412, 2498

[112] Mamon, G., Chevalier, J., Romanovsky, A., Wojtak, R., 2015, IAUS, 311, 16,

[113] Mangano G., Miele, G., Pastor, S., Pinto, T., Pisanti, O., Serpico, P., 2006, NuPhB, 756, 100

[114] Mantz, A., Allen, S., Morris, R., Rapetti, D., Applegate, D., Kelly, P., von der Linden, A.,Schmidt, R., 2014, MNRAS, 440, 2077

[115] Marcovič, K., Viel, M., 2014, PASA, 31, 6

[116] Marsh, D., Silk, J., 2014, MNRAS, 437, 2652

[117] Martinez-Delgado, D., Lasker, R., Sharina, M., et al., 2016, AJ, 151, 96

[118] Mayet, F., Green, A., Battat, J., et al., 2016, PhR, 627, 1

[119] McConnachie, A,, 2012, ApJ, 144, 4

[120] McDonald, M., Benson, B. A., Vikhlinin, A., et al., 2013, ApJ, 774, 23

[121] McLeod, D., McLure, R., Dunlop, J., et al., 2015, MNRAS, 450, 303

[122] Meiksin, A., White, M., Peacock, J., 1999, MNRAS, 304, 851

[123] Merrit, A., van Dokkum, P., Abraham, R., 2014, ApJ, 787, L37

[124] Merten, J., Meneghetti, M.; Postman, M., et al., 2015, ApJ, 806, 4

[125] Mikheeva, E., Doroshkevich A., Lukash, V.,, 2007, NCimB, 122, 1393

[126] Miller, S., Ellis, R., Newman A., Benson, A., 2014, ApJ, 782, 115

[127] Mirizzi, A., Mangano, G., Pisanti, O., Saviano, N., 2015, PhRvD.91.025019

[128] Mitra, S., Choudhury, T.R., Ferrara, A., 2015, MNRAS, 454, L76

[129] Moore, B., Ghigna, S., Governato, F. et al., 1999, ApJ, 524, L19

[130] Moughan, B., Giles, P., Randall, S., Jones, C., Formen, W., 2012, MNRAS, 421, 1583

[131] Nagai, D., Kravtsov, A., Vikhlinin A., 2007, ApJ, 668, 1

[132] Navarro J.F., Frenk C.S., & White S.D.M., 1995, MNRAS, 275, 720

[133] Navarro J.F., Frenk C.S., & White S.D.M., 1996, ApJ, 462, 563

[134] Navarro J.F., Frenk C.S., & White S.D.M., 1997, ApJ, 490, 493

[135] Nesseris, S., Sapone, D., 2015, IJMPD, 24, 1550045

[136] Newman, A., Treu, T., Ellis, R., Sand, D., 2013, ApJ, 765, 25

[137] Nipoti, C., & Binney, J., 2015, MNRAS, 446, 182

[138] Partridge R.B., & Peebles P.J.E., 1967a, ApJ, 147, 868

[139] Partridge R.B., & Peebles P.J.E., 1967b, ApJ, 148, 377

[140] Peebles P.J.E., 1967, ApJ, 147, 859

[141] Peebles P.J.E., 1980, The Large-Scale Structure of the Univers, (Princeton: Princeton Univ. Press)

[142] Penarrubia, J., Navarro, J., McConnachie, A., 2008, ApJ, 673, 226

[143] Penarrubia, J., Benson, A., Walker, M., et al., 2010, MNRAS, 406, 1290

[144] Penarrubia, J., Pontzen, A., Walker, M., Koposov, S., 2012, ApJ, 759L, 42

[145] Pilipenko, S., Doroshkevich, A., Lukash, V., Mikheeva, E., 2012, MNRAS, 427L, 30

[146] Pointecouteau, E., Arnaud, M., Pratt, G., 2005, A&A, 435, 1

[147] Pontzen, A., & Governato, F., 2014, Nature, 506, 171,

[148] Prada, F., Klypin, A., Cuesta, A., et al., 2012, MNRAS, 423, 3018

[149] Pratt, G., Arnaud, M., Pointecouteau, E., 2006, A&A, 446, 429

[150] Pratt, G., Croston, J., Arnaud, M., Böringer, H., 2009, A&A, 498, 361

[151] Pratt, G., Arnaud, M., Piffaretti, R., et al., 2010, A&A, 511, 85

[152] Press, W., Schechter, P., 1974, ApJ, 187, 425

[153] Reichardt, C., Stadler, B., Bleem, L., et al., 2013, ApJ, 763, 127

[154] Robertson, B., Ellis, R., Furlanetto, S., Dunlop, J., 2015, ApJ, 802, L19

[155] Rubakov, V., 2014, Phys. Usp. 57 128

[156] Ruel J., Bazin, G., Bayliss, M., et al., 2014, ApJ, 792,45

[157] Ruffini R., Arguelles, C., Rueda, J., 2015, MNRAS, 451, 622

[158] Saliwanchik, B., Montroy,T., Aird, K., et al. 2015, ApJ, 799, 137

[159] Samushia, L., Reid, B., White, M., et al., 2014, MNRAS, 439, 3504

[160] Saro, A., Liu, J., Mohr, J., et al., 2014,MNRAS, 440, 2610

[161] Savelainen, M., Valiviita, J., Walia, P., et al., 2013, PhRvD., 88, 063010.

[162] Sawala, T., Frenk, C., Crain, R., et al., 2013, MNRAS, 431, 1366

[163] Schewtschenko, J., Baugh, C., Wilkinson, R., et al. 2016, MNRAS, tmp, 862;

[164] Schneider, A., Smith, R., Reed, D., 2013, MNRAS, 433, 1573

[165] Schneider, A., Anderhalden, D., Maccio, A., Diemand, J., 2014, MNRAS, 441, L6

[166] Schultz, C., Onorbe, J., Abazajian, K., Bullock, J., 2014, MNRAS, 442, 1597

[167] Sheth, R., Tormen, G., 2002, MNRAS, 329, 61; 2004, MNRAS, 350, 1385

[168] Suhada, R., et al., 2012, A&A, 537, 39, 1076,

[169] Tasitsiomi, A., Kravtsov, A., Gottlöber, S., Klypin, A., 2004, ApJ, 607, 125

[170] Teyssier, R., Pontzen, A., Dubois, Y., Read, J., 2013, MNRAS, 429, 3068

[171] Tollerud, E., Beaton, R., Geha, M., et al., 2012, ApJ, 752, 45

[172] Tollerud E., Boylan-Kolchin, M., Bullock, J., 2014, MNEAS, 440, 3511

[173] Trujillo-Gomez, S., Klypin, A., Primack, J., Romanowsky, A., 2011, ApJ, 742, 16

[174] Turner, M., Steigmann, G., Krauss, L., 1984, Phys.Rev.Let., 52, 2090.

[175] Umetsu, k., Medezinski, E., Nonino, M., et al., 2014, ApJ, 795, 163

[176] van Dokkum, P., Abraham, R., Merrit, A., et al., 2015, ApJ. 798, L45

[177] van Dokkum, P., Abraham, R., Brodie, J., et al., 2016, ApJ. 828, L6

[178] Viel, M., Becker, G., Bolton, J., Haehnelt,M., 2013, PhRvD, 88d3502

[179] Vikhlinin, A., Kravtsov, A., Forman, W., et al. 2006, ApJ, 640, 691

[180] Vikhlinin, A., Burenin, R., Ebeling, H., et al., 2009, ApJ, 692, 1033

[181] Walker, M., Mateo, M., Olszewski, E., et al. 2009, ApJ., 704, 1274

[182] Walker, M., Penarrubia, J., 2011, ApJ, 742, 20

[183] Wang, M.-Y., Croft, R., Peter, A., Zentner, A., Purcell, C., 2013, PhRvD, 88l3515

[184] Wang, M-Y., Peter, A., Strigari, ., Zentner, A., Arant, B., Garrison-Kimmel, S., Rocha, M., 2014, MNRAS, 445, 614

[185] Weisz, D., et al., 2014, ApJ, 789, 24

[186] Wetzel, A., Deason, A., Garrison – Kimmel, S., 2015, ApJ, 807, 49

[187] Whittaker, L., Brown, M., Battye, R., 2014, MNRAS, 445, 1836

[188] Whittaker, L., Brown, M., Battye, R., 2015, MNRAS, 451, 383

[189] Zel'dovich Ya.B., 1970, A&A, 5, 84

[190] Zel'dovich Ya.B., Novikov I.D., 1983, Structure and evolution of the Universe, University of Chicago Press.

[191] Zhang, Y., Böringer, H., Finoguenov, A., et al., 2006, A&A, 456, 55

[192] Zitrin, A., Labbe, I., Belli, S., et al., 2015, ApJ, 810, L12

[193] Zysina, N., Fomichev, S., Khruschov, V., 2014, PAN, 77, 890